The Astronomical Journal, 137:4377–4399, 2009 May doi:10.1088/0004-6256/137/5/4377

SEGUE: A SPECTROSCOPIC SURVEY OF 240,000 STARS WITH $g = 14$–20

Brian Yanny[1], Constance Rockosi[2], Heidi Jo Newberg[3], Gillian R. Knapp[4], Jennifer K. Adelman-McCarthy[1], Bonnie Alcorn[1], Sahar Allam[1], Carlos Allende Prieto[5,6], Deokkeun An[7], Kurt S. J. Anderson[8,9], Scott Anderson[10], Coryn A. L. Bailer-Jones[11], Steve Bastian[1], Timothy C. Beers[12], Eric Bell[11], Vasily Belokurov[13], Dmitry Bizyaev[8], Norm Blythe[8], John J. Bochanski[10], William N. Boroski[1], Jarle Brinchmann[14], J. Brinkmann[8], Howard Brewington[8], Larry Carey[10], Kyle M. Cudworth[15], Michael Evans[10], N. W. Evans[13], Evalyn Gates[15], B. T. Gänsicke[16], Bruce Gillespie[8], Gerald Gilmore[13], Ada Nebot Gomez-Moran[17], Eva K. Grebel[18], Jim Greenwell[10], James E. Gunn[4], Cathy Jordan[8], Wendell Jordan[8], Paul Harding[19], Hugh Harris[20], John S. Hendry[1], Diana Holder[8], Inese I. Ivans[4], Željko Ivezić[10], Sebastian Jester[11], Jennifer A. Johnson[7], Stephen M. Kent[1], Scot Kleinman[8], Alexei Kniazev[11], Jurek Krzesinski[8], Richard Kron[15], Nikolay Kuropatkin[1], Svetlana Lebedeva[1], Young Sun Lee[12], R. French Leger[1], Sébastien Lépine[21], Steve Levine[20], Huan Lin[1], Daniel C. Long[8], Craig Loomis[4], Robert Lupton[4], Olena Malanushenko[8], Viktor Malanushenko[8], Bruce Margon[22], David Martinez-Delgado[11], Peregrine McGehee[23], Dave Monet[20], Heather L. Morrison[19], Jeffrey A. Munn[20], Eric H. Neilsen, Jr.[1], Atsuko Nitta[8], John E. Norris[24], Dan Oravetz[8], Russell Owen[10], Nikhil Padmanabhan[25], Kaike Pan[8], R. S. Peterson[1], Jeffrey R. Pier[20], Jared Platson[1], Paola Re Fiorentin[11,26], Gordon T. Richards[27], Hans-Walter Rix[11], David J. Schlegel[25], Donald P. Schneider[28], Matthias R. Schreiber[29], Axel Schwope[17], Valena Sibley[1], Audrey Simmons[8], Stephanie A. Snedden[8], J. Allyn Smith[30], Larry Stark[10], Fritz Stauffer[8], M. Steinmetz[17], C. Stoughton[1], Mark SubbaRao[15,31], Alex Szalay[32], Paula Szkody[10], Aniruddha R. Thakar[32], Sivarani Thirupathi[12], Douglas Tucker[1], Alan Uomoto[33], Dan Vanden Berk[28], Simon Vidrih[18], Yogesh Wadadekar[4,34], Shannon Watters[8], Ron Wilhelm[35], Rosemary F. G. Wyse[32], Jean Yarger[8], and Dan Zucker[13]

[1] Fermi National Accelerator Laboratory, P.O. Box 500, Batavia, IL 60510, USA
[2] UCO/Lick Observatory, University of California, Santa Cruz, CA 95064, USA
[3] Department of Physics, Applied Physics and Astronomy, Rensselaer Polytechnic Institute Troy, NY 12180, USA
[4] Department of Astrophysical Sciences, Princeton University, Princeton, NJ 08544, USA
[5] McDonald Observatory and Department of Astronomy, The University of Texas, 1 University Station, C1400 Austin, TX 78712-0259, USA
[6] Mullard Space Science Laboratory, University College London, Holmbury St. Mary, Surrey RH5 6NT, UK
[7] Department of Astronomy, Ohio State University, 140 West 18th Avenue, Columbus, OH 43210, USA
[8] Apache Point Observatory, P.O. Box 59, Sunspot, NM 88349, USA
[9] Department of Astronomy, MSC 4500, New Mexico State University, P.O. Box 30001, Las Cruces, NM 88003, USA
[10] Department of Astronomy, University of Washington, Box 351580, Seattle, WA 98195, USA
[11] Max Planck Institute for Astronomy, Königstuhl 17, D-69117 Heidelberg, Germany
[12] Department of Physics and Astronomy, Center for the Study of Cosmic Evolution, and Joint Institute for Nuclear Astrophysics, Michigan State University, East Lansing, MI 48824, USA
[13] Institute of Astronomy, Madingley Road, Cambridge CB3 0HA, UK
[14] Centro de Astrofísica da Universidade do Porto, Rua das Estrelas, 4150-762 Porto, Portugal
[15] Department of Astronomy and Astrophysics, University of Chicago, 5640 South Ellis Avenue, Chicago, IL 60637, USA
[16] Department of Physics, Warwick University, Coventry CV47AL, UK
[17] Astrophysikalisches Institut Potsdam An der Sternwarte 16, D-14482 Potsdam, Germany
[18] Astronomisches Rechen-Institut, Zentrum für Astronomie, University of Heidelberg, Mönchhofstrasse 12-14, D-69120 Heidelberg, Germany
[19] Department of Astronomy, Case Western Reserve University, Cleveland, OH 44106, USA
[20] US Naval Observatory, Flagstaff Station, 10391 West Naval Observatory Road, Flagstaff, AZ 86001-8521, USA
[21] Department of Astrophysics, American Museum of Natural History, Central Park West at 79th Street, New York, NY 10024, USA
[22] Department of Astronomy and Astrophysics, University of California, 1156 High Street, Santa Cruz, CA 95064, USA
[23] IPAC, MS 220-6, California Institute of Technology, Pasadena, CA 91125, USA
[24] Research School of Astronomy and Astrophysics, Australian National University, Weston, ACT 2611, Australia
[25] Lawrence Berkeley National Laboratory, One Cyclotron Road, Berkeley, CA 94720, USA
[26] Department of Physics, University of Ljubljana, Jadranska 19, 1000 Ljubljana, Slovenia
[27] Drexel University, Philadelphia, PA, USA
[28] Department of Astronomy and Astrophysics, The Pennsylvania State University, University Park, PA 16802, USA
[29] Departamento de Fisica y Astronomia, Facultad de Ciencias, Universidad de Valparaiso, Valparaiso, Chile
[30] Department of Physics and Astronomy, Austin Peay State University, P.O. Box 4608, Clarksville, TN 37040, USA
[31] Adler Planetarium and Astronomy Museum, 1300 Lake Shore Drive, Chicago, IL 60605, USA
[32] Center for Astrophysical Sciences, Department of Physics and Astronomy, Johns Hopkins University, 3400 North Charles Street, Baltimore, MD 21218, USA
[33] Observatories of the Carnegie Institution of Washington, 813 Santa Barbara Street, Pasadena, CA 91101, USA
[34] National Centre for Radio Astrophysics, Post Bag 3, Ganeshkhind, Pune 411007, India
[35] Department of Physics, Texas Tech University, Lubbock, TX, USA

Received 2008 September 29; accepted 2009 February 8; published 2009 April 7

ABSTRACT

The Sloan Extension for Galactic Understanding and Exploration (SEGUE) Survey obtained ≈240,000 moderate-resolution ($R \sim 1800$) spectra from 3900 Å to 9000 Å of fainter Milky Way stars ($14.0 < g < 20.3$) of a wide variety of spectral types, both main-sequence and evolved objects, with the goal of studying the kinematics and populations of our Galaxy and its halo. The spectra are clustered in 212 regions spaced over three quarters of the sky. Radial velocity accuracies for stars are $\sigma(\mathrm{RV}) \sim 4$ km s^{-1} at $g < 18$, degrading to $\sigma(\mathrm{RV}) \sim 15$ km s^{-1} at $g \sim 20$. For stars with signal-to-noise ratio >10 per resolution element, stellar atmospheric parameters are

estimated, including metallicity, surface gravity, and effective temperature. SEGUE obtained 3500 deg^2 of additional *ugriz* imaging (primarily at low Galactic latitudes) providing precise multicolor photometry ($\sigma(g, r, i) \sim 2\%$), ($\sigma(u, z) \sim 3\%$) and astrometry ($\approx 0''.1$) for spectroscopic target selection. The stellar spectra, imaging data, and derived parameter catalogs for this survey are publicly available as part of Sloan Digital Sky Survey Data Release 7.

Key words: Galaxy: halo – Galaxy: stellar content – Galaxy: structure – stars: abundances – stars: fundamental parameters – stars: general

Online-only material: color figure, machine-readable and VO tables

1. INTRODUCTION

1.1. Stellar Spectroscopic Surveys

A large-scale study of the Milky Way is important to our general understanding of galaxy structure and formation. It is only in our own "backyard" that great numbers of stars, the building block of all galaxies, may be observed individually, with their collective properties serving as constraints on theories of galaxy formation and evolution. Spectroscopic data of individual stars can provide a much richer variety of information on both stellar kinematics and stellar atmospheric parameters than is possible with photometric measurements alone.

The first large area spectroscopic surveys used objective prism plates, including the fundamental surveys for spectroscopic classification (Cannon & Pickering 1918; Morgan et al. 1943; Houk 1978) and more specialized surveys for unusual stars (Cameron & Nassau 1956; Nassau et al. 1965; Slettebak & Brundage 1971; Bidelman & MacConnell 1973). Later objective prism surveys focused on extremely metal-poor stars (Beers et al. 1985; Christlieb et al. 1999) and on halo giants (Ratnatunga & Freeman 1985; Flynn & Morrison 1990). Objective prism surveys had the advantage of rapidly recording a large number of stellar spectra over significant solid angles, but had disadvantages such as a bright limiting magnitude and an inability to accurately calibrate the spectra.

"Aperture" spectroscopic surveys using modern spectrographs have been rarer, in part because of the huge investment of telescope time required to assemble substantial-sized samples. They include the "Spaghetti" survey for halo giants (Morrison et al. 2000), the SIM Grid Giant Star Survey (Patterson et al. 1999), the detailed chemical study of Edvardsson et al. (1993) and its various sequels, and the monumental survey of Nordström et al. (2004) who studied nearby, bright F and G stars and obtained metallicity, temperature, and age information from Strömgren photometry and accurate radial velocities (RVs) from CORAVEL and other spectrographs.

Multi-object spectroscopic surveys (first implemented with plug boards, or slit masks, then with automated positioners), which provide a large gain in efficiency, have also been done with specific scientific goals in mind. A number of programs (Kuijken & Gilmore 1989; Ibata & Gilmore 1995; Ibata et al. 1994; Gilmore et al. 1995, 2002) have searched for coherent structures in the halo. The RAVE Survey (Steinmetz et al. 2006; Zwitter et al. 2008), which focuses on bright stars of all colors ($9 < I < 13$), produces accurate velocities and estimates of stellar parameters from a small spectral region including the Ca II infrared (IR) triplet.

Orthogonal to the volume-limited or spectral-type specific surveys have been the compilations of homogeneous spectroscopic atlases of a few hundred objects (Gunn & Stryker 1983; Jacoby et al. 1984; Pickles 1985) obtained with electronic scanners and imaging tubes. The members of these catalogs were selected to sample objects of all spectral types with at least one example of each temperature and luminosity class. These catalogs do not give relative numbers of stars in the different spectral categories, however, and they may miss some rare categories, especially the low-metallicity stars.

Looking to the future, the Gaia space-based mission (Perryman et al. 2001) plans to obtain proper motions (and precise positions) of approximately one billion stars to $g \sim 20$, with radial velocities (RVs) for all of the brighter objects with $g < 17$ (Katz et al. 2004; Wilkinson et al. 2005). Gaia, when underway, will represent a several orders of magnitude leap forward in our knowledge of the kinematics, structure, and evolution of our Galaxy.

1.2. Stars and the SDSS

The Sloan Digital Sky Survey (SDSS; York et al. 2000) is primarily an extragalactic survey that has obtained 2% multicolor imaging of nearly 8000 deg^2 of filled contiguous sky toward the Northern Galactic Cap, and 700 deg^2 in three stripes in the South Galactic Cap near the celestial equator. Spectra have been acquired of one million galaxies and one hundred thousand quasars. The major science program consists of constructing a large three-dimensional map of the universe and constraining cosmological models; see, e.g., Becker et al. (2001), Blanton et al. (2003b), Fan et al. (2003), Tremonti et al. (2004), Tegmark et al. (2004), Eisenstein et al. (2005), and Richards et al. (2006).

A significant product of the SDSS was a large number of Milky Way stellar spectra combined with deep, accurate multicolor photometry. This led to several (initially) serendipitous Galactic structure, Galactic halo, and M31 halo science results; see Ivezić et al. (2000), Yanny et al. (2000, 2003), Newberg et al. (2002, 2003), Rockosi et al. (2002), Willman et al. (2005), Zucker et al. (2004a, b), Belokurov et al. (2006a, b, 2007a, b), Allende Prieto et al. (2006), Bell et al. (2008), Koposov et al. (2007), Xu et al. (2007), Xue et al. (2008), and Juric et al. (2008).

Near the conclusion of the original SDSS program in 2004, partially as a result of the productive Galactic science enabled by the SDSS, a set of three individual surveys (under the umbrella designation of SDSS-II) were designed: (1) Legacy: a survey following the same goals of the original SDSS, to complete the SDSS imaging and spectroscopic footprint; (2) SN Ia (Frieman et al. 2008): a well-calibrated, systematic survey for 200 intermediate redshift ($0.1 < z < 0.4$) type Ia supernovae, filling an important gap in redshift coverage, and anchoring the calibrations of higher redshift supernova surveys; and (3) Sloan Extension for Galactic Understanding and Exploration (SEGUE), an imaging and spectroscopic survey of the Milky Way and its surrounding halo. SDSS-II operated from 2005 August to 2008 July at Apache Point Observatory, building on SDSS, which is operated from 2000 August until 2005 July.

The SEGUE Survey is the subject of this paper. The processed, searchable data archive from SEGUE was made publicly available in the Fall of 2008 as part of SDSS-II Data Release 7 (DR7). With few exceptions, all stellar spectral types are represented in the SEGUE Survey. Notable categories which are missing include luminous Population I early types, such as O, B, and Wolf–Rayet stars, and some Population I giants, which are not targeted because they are generally too bright for SEGUE observations if they are in the solar neighborhood and are too rare or are obscured by dust toward the Galactic center to be seen at greater distances. Samples of spectrophotometrically calibrated stars of a wide variety of spectral types are presented in Section 3. A defining part of SEGUE is the creation and release of its public database that can be mined to enable a whole range of astrophysics projects not conceived of when the survey was carried out.

2. SURVEY GOALS AND FOOTPRINT

2.1. SEGUE Goals

The original, five-year SDSS program demonstrated the existence of significant spatial substructure in the stellar halo of the Milky Way discovered from photometric data, from which stellar distance estimates were obtained primarily for bluer (A and F) stars. These substructures cast doubt upon previous measurements of a presumed axially symmetric spheroid stellar component of the Galaxy with a smoothly varying power-law density structure. Discovery of the substructure also created a tremendous need for follow-up spectroscopy of each structure, so that stellar population and orbital information for the debris could be determined.

SEGUE was designed to sample the stellar spheroid at a variety of distances, from a few kpc to a hundred kpc, in 200 "pencil beams," spaced around the sky so that they would intersect the largest structures. At the time SEGUE was designed, we knew about the Sagittarius Dwarf spheroidal tidal debris stream and the controversial Monoceros stream in the Galactic plane. Both structures were 6–10 kpc across and were believed to extend all of the way around the Milky Way. We expected that additional substructure would be discovered, and that it was most important to identify and characterize the largest structures; without knowledge of the spatial variation of the spheroid at 10 kpc scales, it was difficult to positively identify smaller or lower surface brightness structures.

SEGUE augmented the photometric data from the SDSS/Legacy Surveys to sample the sky about every 15° across the sky, in all parts of the sky accessible from the telescope's latitude. This included adding photometry at low latitudes ($|b| < 35°$) and additional photometry in the South Galactic Cap. Two hundred pencil beams were selected for spectroscopy because these could be arranged to sample the sky at intervals of 10°–15°, and two observations of each pencil beam could be observed in the three-year duration of SDSS-II.

Spectroscopic target selection was designed to maximize the science from SEGUE stellar spectroscopy; in particular, we wished to study the Milky Way's chemical and dynamic formation history and to constrain the Galaxy's gravitational potential.

The target-selection strategy that was used to achieve these general goals devoted most of the fibers on each pencil beam line of sight to sampling the stellar populations of the Galaxy on large (tens of kpc) scales, including spheroid substructure and global properties of the thin and thick disk components. In addition, a small subset of the fibers was devoted to unusual stars, including those thought to have low metallicity ([M/H] < -2) or to be otherwise unusual based on their colors and velocities (as determined by photometry and proper motions). In addition, we specifically targeted star clusters with a variety of ages and metallicities so that this important spectral database could be well calibrated.

To meet these goals, SEGUE has produced (1) an imaging survey of 3500 deg^2 of *ugriz* imaging with the SDSS telescope and camera (Gunn et al. 1998, 2006), (2) a spectroscopic catalog that spans the stellar population observable in magnitude and Galactic latitude range of the data at a resolution of $R \sim 1800$. The spectroscopic catalog includes estimates for the observational parameters (position, RV, multicolor photometric, and spectrophotometric magnitudes), as well as the derived, modeled parameters (including [M/H], surface gravity, and $T_{\rm eff}$) for all observed stars in a systematic and well-calibrated fashion.

2.2. SEGUE Imaging

The original SDSS imaged most of the North Galactic Cap plus three stripes of data in the South Galactic Cap; regions of low Galactic latitude ($|b| < 35°$) were largely excluded by design. The SEGUE imaging footprint was designed to allow the selection of spectroscopic targets in as broad a range of sky directions as possible, to enable study of the important transition zones between our Milky Way's disks and stellar halo, to include a large and varied sample of Galactic star clusters that could be used for calibration, and to ensure that photometric calibration would be feasible (i.e., avoid zones of extreme and variable extinction).

The low-latitude SEGUE imaging area includes 15 2.5-wide stripes of data along constant Galactic longitude, spaced by approximately 20° around the sky. These stripes probe the Galaxy at a wide variety of longitudes, sampling the changing relative densities of global Galactic components (thin disk, thick disk, halo). The precise longitudes of the SEGUE stripes are not evenly spaced; the l of several stripes were shifted by up to 8°, so that several known open clusters near the Galactic plane could be optically imaged. We added two stripes of data in the South Galactic Cap. Because spectra of stars toward cardinal Galactic directions (l near 90°, 180°, 270°, 360°) are important for generating a simplified kinematic analysis of a very complex dynamic Galaxy, the two SEGUE stripes (at $l = 94°$ and $l = 178°$) that nearly coincide with cardinal pointings were extended to give nearly complete pole-to-pole imaging and more complete spectroscopic plate coverage than at other longitudes. Where possible, the SEGUE stripes were designed to cross other SDSS imaging data at multiple locations to facilitate photometric calibration.

Figure 1 shows the constant longitude and two Southern imaging stripes chosen to augment the original SDSS footprint in the Equatorial (top) and Galactic coordinates (bottom). We sample the sky in all directions that are accessible to the Apache Point Observatory; since the observatory is at a Northern latitude of 32°, essentially no SEGUE data is obtained with the Equatorial coordinates $\delta < -20°$. The Galactic anticenter ($\delta = 29°$) is well sampled, but the Galactic center ($\delta = -29°$) is not. The stellar population of the bulge is largely inaccessible and obscured by dust in this optical survey.

The SEGUE imaging scans (i.e., data not associated with the Legacy SDSS Survey) are tabulated in Table 1. All SEGUE imaging was obtained between 2004 August and 2008 January.

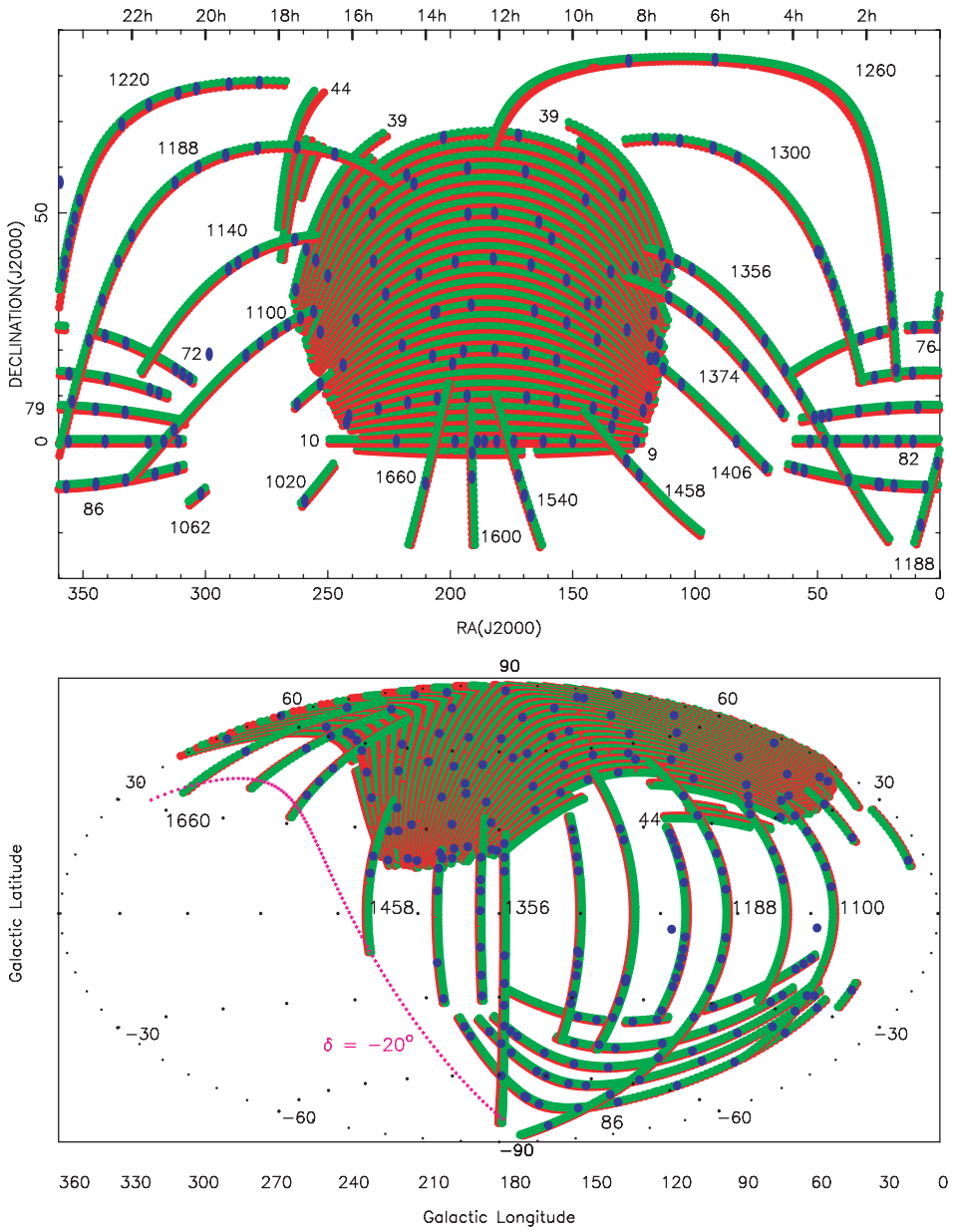

Figure 1. SEGUE Survey footprint—Upper panel: the SEGUE Survey footprint in the equatorial coordinates from 360° to 0° (left to right) and −26° to 90° (bottom to top). Selected stripes are labeled with their stripe number. The SDSS North Galactic Cap stripes are numbered from 9 to 44. Southern SDSS stripes are numbered 76, 82, and 86. SEGUE fills in Southern stripes 72 and 79. SEGUE's constant Galactic longitude stripes are numbered with *stripe* = 1000 + 2*l* where *l* is the Galactic longitude. Each SEGUE plate pointing (usually representing a pair of 640 hole plates), is indicated with a blue circle. Lower panel: the SEGUE Survey (l, b) in Aitoff projection, centered on the Galactic anticenter. The line marking the Southern limit of the telescope observing site $\delta = -20°$ is indicated in magenta. Red and green filled areas represent South and North SDSS and SEGUE strips, respectively.

(A color version of this figure is available in the online journal.)

Note that each SEGUE stripe is 2.°5 wide. Stripes 72 and 79 follow standard numbering conventions of the original SDSS imaging survey. Stripes with four-digit numbers run along constant l, running for variable extents in b. The formula for converting the SDSS Survey coordinates (μ, ν) for a particular node and inclination to the equatorial coordinates J2000 (α, δ) may be found in Stoughton et al. (2002).

Except in regions of high stellar density, the processing and calibration of the SEGUE imaging data are the same as that of the SDSS imaging data (Blanton et al. 2003a; Fukugita et al. 1996; Hogg et al. 2001; Pier et al. 2003; Smith et al. 2002; Stoughton et al. 2002; Tucker et al. 2006). A modified version of the SDSS PHOTO processing pipeline software (R. H. Lupton et al. 2010, in preparation) was combined with the Pan-STARRS (Magnier 2006) object-detection code, and was run on all lower latitude SEGUE imaging scans. The key modifications were (1) the PHOTO code was optimized for primarily stellar objects by truncating fits to the wings of extended sources at essentially the point-spread function (PSF) radius, (2) the PHOTO code's object deblender was allowed to deblend groups of closely spaced objects into more "child" objects than in standard high-latitude (less crowded) SDSS fields, and (3) Pan-STARRS threshold object-detection code was used. This code generates more complete object lists in regions of high stellar density, and was used to supplement PHOTO's object detector. Imaging scans which participated in

Table 1
SEGUE Imaging Area Stripes[a]

Stripe[b]	l (°)	Node (°)	Incl.[c] (°)	μ_{start}[d] (°)	μ_{end} (°)	b_{start} (°)	b_{end} (°)	Area (deg^2)
72	...	95.000	−25.000	311.0	419.0	−14.9	−27.1	270.0
79	...	95.000	−7.500	311.0	419.0	−22.4	−35.3	270.0
1020	10	60.004	34.950	242.3	277.3	35.0	0.0	87.5
1062	31	98.629	27.192	247.4	312.4	35.0	−30.0	162.5
1100	50	136.813	31.702	252.0	332.0	35.0	−45.0	200.0
1140	70	161.744	44.754	257.1	337.1	35.0	−45.0	200.0
1188	94	178.713	64.498	249.1	384.1	50.0	−85.0	337.5
1220	110	186.882	78.511	269.6	349.6	35.0	−45.0	200.0
1260	130	196.095	276.287	33.8	128.8	−45.0	50.0	237.5
1300	150	205.976	293.890	41.1	121.1	−45.0	35.0	200.0
1356	178	225.998	316.856	14.2	129.2	−80.0	35.0	287.5
1374	187	236.019	323.166	66.5	131.5	−30.0	35.0	162.5
1406	203	261.852	331.241	70.5	135.5	−30.0	35.0	162.5
1458	229	315.139	328.784	94.8	146.8	−12.0	40.0	130
1540	270	176.405	61.064	152.8	187.8	35.0	70.0	87.5
1600	300	191.522	87.391	171.7	198.7	43.0	70.0	67.5
1660	330	25.976	66.110	195.0	230.0	38.0	70.0	80.0

Notes.
[a] Each great-circle scan of the SDSS camera is designated as a strip. Given the gaps between the CCDs in the camera, the 2.°5-wide region in the focal plane must be imaged with two scans to completely cover the area. The filled 2.°5 region is called a stripe (see Stoughton et al. 2002).
[b] Stripes numbered below 1000 are part of the Legacy Survey, those numbered above 1000 are special SEGUE stripes (as can be seen by the fixed Galactic longitudes of the SEGUE stripes).
[c] Inclination of stripe relative to the celestial equator, node is at $\alpha = 95°$ for SDSS (non-SEGUE) stripes.
[d] μ is the analog of right ascension in the great-circle coordinate system, ν is the analog of declination.

this low-latitude processing are tagged in the data archive with a rerun (reprocessing version) number of 648. This is in contrast to standard SDSS and SEGUE PHOTO reprocessing numbers $40 \leqslant$ rerun $\leqslant 44$. Except in regions of high stellar density, the magnitudes from this version of PHOTO are interchangeable (within the errors) with the version used to process the rest of the SDSS and SEGUE imaging data. At high stellar density the choice depends on the needs of the particular investigation. Both the PHOTO PSF magnitudes and the Pan-STARRS aperture magnitudes are available for comparison in the DR7 data archive for low-latitude regions of sky. We refer the reader to the DR7 paper (Abazajian et al. 2009) for more discussion of this reprocessing of the imaging data, and to the documentation on the DR7 Web site. At the density extreme, several globular clusters present in the SDSS and SEGUE footprints are analyzed by An et al. (2008) using independent software (see below).

As in SDSS DR6 (Adelman-McCarthy et al. 2008), the zeropoint photometric calibration SEGUE imaging has been enhanced by the calibration procedure described in Padmanabhan et al. (2008). This procedure finds a simultaneous global fit for the individual imaging scans' photometric zeropoints, extinction coefficients, and flat-field characteristics (of all 30 SDSS camera CCDs), relying on the overlap between SEGUE and SDSS Legacy scans to improve the absolute zeropoints accuracies in the gri filters to <1% in most areas around the sky.

2.3. SEGUE Spectroscopy

SEGUE leveraged the unique features of the SDSS telescope and spectrographs (namely the ability to go deep and wide, with broad spectral coverage and high spectrophotometric accuracy) to acquire spectra of ∼240,000 stars of a wide variety of spectral types (from white dwarfs (WDs) on the blue end to M and L subdwarfs on the red end), probing a wide range of distances (less than 10 pc to greater than 100 kpc). The SDSS spectrographs used for SEGUE are a pair of highly efficient dual CCD camera, fiber-fed spectrographs, with wavelength coverage from 3900 Å to 9000 Å at resolving power $R \sim 1800$. The twin spectrographs can simultaneously record data from 640 fibers in a 7 deg^2 field of view; 7%–12% of the fibers are reserved for sky signal and other calibration fibers (such as spectrophotometric standard stars, generally chosen from color-selected F subdwarfs with $16 < g < 18.5$).

SEGUE took spectra of stars in the magnitude range $14 < g < 20.3$. At $g \sim 14$, the SDSS spectrographs saturate in a 300 s exposure. Objects down to $r = 18.5$ can be routinely obtained with signal-to-noise ratio (S/N) > 30, sufficient for RVs good to 4 km s^{-1} and metallicity [M/H] measurements accurate to 0.2 dex for a wide variety of spectral types (A–K). At $g \sim 20.3$, we were able to obtain S/N ∼ 3 in 2 hr integration time under photometric conditions with seeing of 2″ or better (all S/N quotations are per 150 km s^{-1} resolution element).

Spectroscopic plate pointings sparsely sample all areas of the sky with available imaging (Figure 1), probing all the major known Galactic structures (thin and thick disk, halo, and streams) with the exception of the bulge, which is below our Southern declination limit. To study the detailed structure of these Galactic components, the density of targets is made high enough that the velocity distribution of one homogeneous subset of stars (the G dwarfs) in one distance bin (an interval of one apparent magnitude) may be determined to be either consistent or distinct from a Gaussian. This requires at least 40 targets of one spectral type (G dwarfs) per magnitude interval (14th through 20th) per plate pointing. It is this scientific goal which drives the assignment of over 300 fibers per plate pair to G star candidates toward each SEGUE line of sight.

The required RV accuracy is driven by the scientific goal of separating stellar streams with dispersion $\sigma \sim 10$ km s^{-1} from field disk and halo stars with dispersions of $\sigma \sim 30$ and 100 km s^{-1}, respectively. Figure 2 shows the actual relative RV accuracy obtained from SEGUE spectra using quality assurance (QA) stars. These are simply stars at $r \sim 18$ that are observed twice, once on each of the two plates that make a complete observation of a SEGUE pencil beam. There are ∼20 such pairs for every pencil beam. We restrict our QA sample to those with S/N > 10. RVs are measured by cross-correlating each spectrum against a set of ∼900 selected templates taken from the ELODIE high-resolution spectroscopic survey (Moultaka et al. 2004). The ELODIE templates span a wide range of spectral types and metallicities. Very early and very late types, however, are nearly absent. We note that the correlation is done by shifting each spectrum repeatedly, stepping through wavelength space (rather then via fast Fourier transform techniques), and, while time consuming, this appears to result in somewhat higher accuracy. The top panel shows the measured RV difference histogram between all QA stars and a second observation of the same stars on a different plate. Individual errors are $\sigma \sim 4.4$ km s^{-1}. The lower panel shows how the RV accuracy degrades with color and S/N: in general bluer objects have worse RV errors than red, with blue horizontal branch stars (BHBs) and their broad Balmer lines being hardest to measure accurately. We expand on the content of Figure 2 in Table 2, where we order the set of spectra with multiple independent

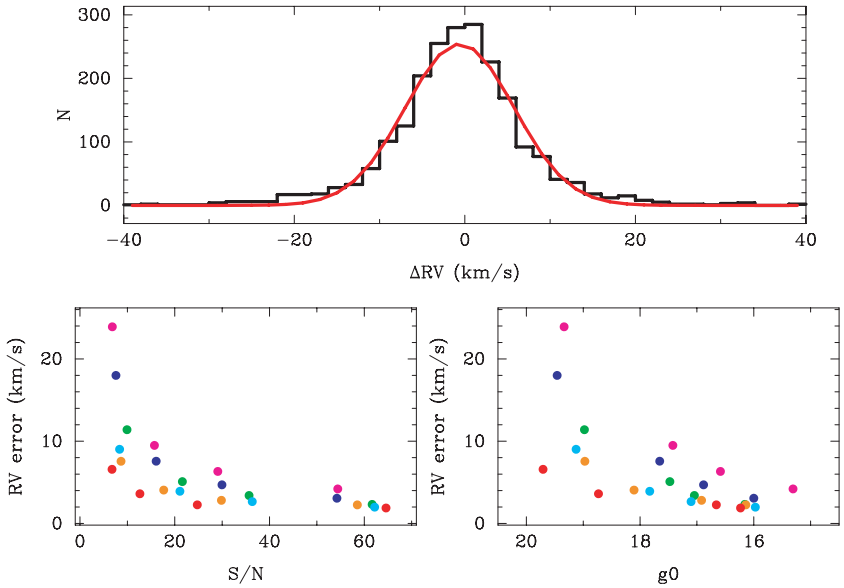

Figure 2. SEGUE RV accuracy—the top panel shows the histogram of differences in spectroscopic pipeline measurements of RV for two separate observations of the same star on different survey SEGUE plates for 2200 stars with $r \sim 18$ and S/N > 10. The quoted sigma is divided by $\sqrt{2}$ to estimate the measurement error for a single observation. The red curve is the best-fit Gaussian, it has a mean offset of <0.3 km s^{-1} and a $\sigma/\sqrt{2} = 4.4$ km s^{-1}. Lower panel: RV accuracy by S/N and $(g-r)_0$ color. The color code is magenta: $(g-r)_0 < 0.1$ (BHB/BS/A), blue: $0.1 < (g-r)_0 < 0.3$ (F), green: $0.3 < (g-r)_0 < 0.48$ (F/G), cyan: $0.48 < (g-r)_0 < 0.55$ (G), orange: $0.55 < (g-r)_0 < 0.75$ (G/K), and red: $0.75 < (g-r)_0 < 1.0$ (K).

Table 2
Velocity Errors by Color and S/N Quartile

$(g-r)_0$ (mag)	N	$\bar{g}_0$	Q1 (S/N)	σ (km s^{-1})	$\bar{g}_0$	Q2 (S/N)	σ (km s^{-1})	$\bar{g}_0$	Q3 (S/N)	σ (km s^{-1})	$\bar{g}_0$	Q4 (S/N)	σ (km s^{-1})
$(g-r)_0 < 0.10$	488	19.3	6.8	23.9	17.4	15.7	9.5	16.6	29.1	6.3	15.3	54.4	4.2
$0.1 < (g-r)_0 < 0.30$	2504	19.5	7.6	18.0	17.7	16.1	7.6	16.9	30.0	4.7	16.0	54.2	3.1
$0.3 < (g-r)_0 < 0.48$	2600	19.0	9.9	11.4	17.5	21.6	5.1	17.0	35.7	3.4	16.2	61.7	2.3
$0.48 < (g-r)_0 < 0.55$	4348	19.1	8.4	9.0	17.8	21.1	3.9	17.1	36.4	2.7	16.0	62.2	2.0
$0.55 < (g-r)_0 < 0.75$	2260	19.0	8.7	7.6	18.1	17.7	4.1	16.9	29.9	2.8	16.1	58.5	2.3
$0.75 < (g-r)_0 < 1.00$	700	19.7	6.7	6.6	18.7	12.6	3.6	16.7	24.8	2.8	16.2	64.6	1.9

observations of the same object by S/N and divide the data for each of the six color ranges into four quartiles. For each color range from blue to red, we tabulate N and list by quartile the average (dereddened) magnitude $\bar{g}_0$, average S/N, and the 1σ velocity error (divided by $\sqrt{2}$ to compensate for the fact that we have two independent measurements). The errors are well behaved as S/N decreases from >50 to <10. We do not characterize velocity errors for extreme spectral types (WDs on the blue end and late M and L type stars on the red end), as these samples have very large systematic errors, due to very broad spectral features and a lack of standard templates with which to cross-correlate. Follow-up reductions of the SEGUE spectra will include synthetic templates for deriving velocities for stars with unusual Carbon enhancement (S. Thirupathi 2008, private communication).

One component of the total RV error is the systematic error in zeropoint of each plate. The scatter in that offset between plates, measured from the mean offset of the QA stars for each pencil beam, has zero mean and standard deviation 1.8 km s^{-1}. This scatter of 1.8 km s^{-1} contributes to the RV uncertainty of all SEGUE stars, and sets the lower bound of our RV errors. To check the overall zeropoint of the RV calibration we used a set of 100 bright field stars observed both with SEGUE and at higher resolution on the Hobby-Eberly telescope (Allende Prieto et al. 2008). SEGUE spectra of stars in the outskirts of globular clusters with known RV also provided checks on the RV zeropoint. This analysis resulted in an offset of 7.3 km s^{-1} with very small scatter. This 7.3 km s^{-1} offset was applied to SEGUE RVs (but not to the z redshift measurements directly from the spectroscopic pipelines) in the final DR7 catalog. The origin of these systematics are not completely understood, but they are thought to be associated with telescope flexure or night sky line fitting errors when computing wavelength solutions for each merged SEGUE plate, which consists of a numbers of exposures taken over several hours, often spanning multiple nights (see below).

Our scientific goals require that for a large fraction of the stars with $g < 18.5$, sufficient S/N be obtained so it is possible to reliably estimate the metallicities [M/H] and luminosity classes (dwarf vs. subgiant vs. giant) for stars of spectral types A–M well enough to separate stream stars from field disk populations from halo populations. An S/N > 10 is required to measure these stellar atmospheric parameters, with more accurate measurements at higher S/N. This drove the integration time for the SDSS spectrographs to about 2 hr for a $g = 18.5$ object and 1 hr for a $g = 17$ object.

The actual SEGUE spectroscopic survey selected pointings are shown as blue circles in Figure 1. There are 212 SEGUE pointings on the sky, all listed in Table 3. These pointings are divided into the following categories: (1) "Survey," 172

Table 3
List of SEGUE Plate Pairs

pid	bplate	fplate	bmjd	fmjd	stripe	α_{J2000}	δ_{J2000}	l	b	$E(B-V)$	Version	Category
153	2668	2672	54084	54085	1374	79.49	16.61	187.00	−12.00	0.46	v4.2	LLSurvey
065	2300	2302	53682	53709	1300	82.64	62.07	150.00	15.00	0.25	v3.2	Survey
040	2052	2072	53401	53430	82	83.20	0.00	203.68	−17.42	0.26	v3.0	Survey
231	*2887	2912	54495	54499	1374	91.30	23.40	187.00	1.00	0.77	v4.6	Calib Cluster
133	2540	2548	54110	54152	1260	91.83	83.51	130.00	25.71	0.06	v4.0	Survey
064	2299	2301	53711	53712	1300	92.63	64.25	150.00	20.00	0.11	v3.2	Survey
260	2941	2946	54507	54506	38	111.29	37.62	180.89	22.44	0.05	v4.6	Mon Strm
036	2053	2073	53446	53728	37	112.51	35.99	182.90	22.87	0.06	v3.0	Survey

Notes.
* Plate obtained in bright moon, velocities off by up to 10 km s^{-1}.

(This table is available in its entirety in machine-readable and Virtual Observatory (VO) forms in the online journal. A portion is shown here for guidance regarding its form and content.)

approximately evenly spaced pointings around the SDSS and SEGUE imaging area, separated by no more than 20° from the next nearest pointing, sampling all directions without regard for known structures or streams; (2) "LLSurvey," 12 pointings at low latitude, where a separate target-selection algorithm is used that functions even in highly reddened lines of sight; (3) "Strm," 16 pointings toward five previously discovered stream-like structures around the halo of the Milky Way, such as the Sagittarius or Orphan streams; (4) "Cluster," 12 pointings toward known globular or open clusters of known [M/H] for purposes of calibrating the metallicity and luminosity pipelines; and (5) "Test," five early SEGUE pointings to test the target-selection algorithms at a variety of latitudes and to test the RV accuracy of the survey. Six pointings are duplicated. Note that a significant fraction of SEGUE spectroscopy relies upon the SDSS Legacy Survey imaging in the North Galactic Cap.

A SEGUE (and SDSS) spectroscopic plate is a circular disk of machined aluminum, with a diameter of 0.75 m, corresponding to an angular on-the-sky radius of 1.°49. A small hole, holding one fiber, is drilled at the position of each object of interest. Each plate may have up to 640 object holes, which are fed to twin 320-fiber spectrographs. Target holes are restricted to being no closer together than 55″ on the sky (Stoughton et al. 2002). The total area of each plate is approximately 7 deg^2 on the sky.

Because there are many more than 640 stars per 7 deg^2 to $g = 20.3$ and because the SEGUE magnitude limits $14 < g < 20$ span more than a factor of 100 in apparent brightness, we observe each SEGUE pointing with two SDSS-style plates, each with a maximum of 640 fibers. Recall that for SDSS extragalactic observations, only one plate at each position was designed, to match the sampling of approximately 100 galaxies per square degree for objects with $r_{extended} < 17.77$.

One plate of the pair is called the SEGUE bright (or SEGUE regular) plate, and consists of holes targeting stars with $14.0 < r < 17.8$, exposed for typically 1 hr. The bright magnitude limit is set by the saturation of the spectrographs for a 300 s exposure, as well as cross-talk considerations between the brightest and faintest objects in adjacent fibers on a given plate. The second plate of 640 fibers, designated the SEGUE faint plate, primarily consists of stars with $17.8 < r < 20.1$, exposed for a total of typically 2 hr.

About 20 stars per pointing with $r \sim 18$ are targeted twice, on both the bright and faint plates. These objects are called QA objects, and, as mentioned above, are used to determine the systematic reproducibility of RVs and other derived parameters from plate to plate.

For the special case of "Cluster" plates, where it is desired to obtain spectra of bright nearby globular cluster giant branch stars for calibration, the SDSS spectrograph saturation limit is extended by taking short (1–2 minute) exposures, allowing one to sample stars as bright as $g \sim 11$. These short exposures, however, have little sky signal, and it is thus difficult to do an accurate wavelength calibration. This is because the final step in the calibration process depends on using the positions of fixed, known night sky lines such as Hg, Na, and [O I].

The bright plates have 32 fibers reserved for blank sky and 16 reserved for spectrophotometric standards; the faint plates have 64 fibers reserved for blank sky and 16 fibers reserved for spectrophotometric standards. This approach leaves approximately 1152 fibers available for science targets in each 7 deg^2 pointing. The number of sky fibers was determined by the need to maximize target S/N in fiber-fed multi-object spectrographs, as discussed in Wyse & Gilmore (1992). The spectrophotometric standards (primarily halo F subdwarfs) from SEGUE and the SDSS Survey constitute a valuable sample in themselves for numerous Galactic structure studies (Allende Prieto et al. 2006; Carollo et al. 2007).

Altogether, there are 416 plates in the SEGUE database; all but 17 of the 212 SEGUE pointings have a bright and faint plate of ∼576 targets each. Individual 10–30 minute exposures were obtained, sometimes on successive nights, until the desired S/N for each SEGUE plate was reached. All common exposures for a given plate and plugging (fibers are plugged into the metal plates by hand and the plugged plates can be moved into and out of the focal plane as many times as necessary to reach a desired S/N value) were combined and uniquely identified by four-digit plate number and by the Modified Julian Date (MJD) of the last night on which a given plate–plugging was observed. The plate names and identifying observation dates (MJDs) are all in Table 3. The total number of unique SEGUE spectra is approximately 240,000.

SEGUE spectra are processed with the same basic pipelines used to process the SDSS data (Stoughton et al. 2002). The pipelines have been modified slightly to enhance the RV accuracy of stellar spectra. It should be noted that a handful of SEGUE plates were obtained under moon illumination fractions of greater than 0.85, and a careful analysis indicates that the wavelength solutions of these 10 plates are systematically off by as much as 10 km s^{-1}. These plates are marked in Table 3 with asterisks.

In addition to the standard extraction and RV reduction pipelines of SDSS, the SEGUE plates have been processed through an additional "SEGUE Stellar Parameters Pipeline"

Table 4
SSPP Flags

Flag	Meaning
n	All is normal for this flag position
d	Possible WD
D	Apparent WD
E	Emission, possible QSO
h	Helium line detected
H	Apparent Teff too Hot for parameter est.
l	Sodium line, possibly late type
N	Noise spectrum
S	Sky fiber—no signal
V	RV mismatch
C	Color mismatch (spectroscopic color Teff far from implied $(g-r)_0$ color Teff)
B	Balmer flag: unusual Balmer eq. widths for star
g	g band: unusual G-band eq. width for star–Carbon star?
G	Carbon star?

(SSPP) that estimates the metallicity [M/H], surface gravity ($\log g$), and effective temperature $T_{\rm eff}$, along with associated errors, for each star with sufficient S/N. Details of the design, operation, and error analysis of the SSPP as run on SEGUE spectra are described in Lee et al. (2008a, 2008b) and Allende Prieto et al. (2008). The uncertainties in the SSPP parameters were determined by analysis of star clusters with known metallicities, reddenings, and distances and by comparison of SSPP-derived parameters with parameters derived from higher resolution spectra of the same sample of field stars. For spectra with S/N $>$ 30, which are usually obtained for stars with $g <$ 18.5, the errors are $\sigma([{\rm M/H}]) \sim 0.2$ dex, $\sigma(\log g) \sim 0.3$ dex, and $\sigma(T_{\rm eff}) \sim 200$ K. These uncertainties are valid for stars with $T_{\rm eff}$ between 4500 K and 8500 K. For stars outside this temperature range, and for stars of lower S/N, atmospheric parameters are still computed, but with appropriately higher error estimates. Table 4 contains a list of SSPP quality flags which are set for every spectrum. These flags, when set, indicate something unusual about a given spectrum, i.e., one with unusually strong Balmer, Mg or Na lines, or one where there is a mismatch between the photometric color (derived from the $(g-r)_0$ color), and the spectroscopic type of the star. Within the context of DR7, a practical quality cut used to select only stars (and avoid galaxies, quasars, and low-S/N spectra of the sky) is to insist that a given spectrum has the error on the ELODIE template cross-correlation RV *elodierverr* strictly > 0.

3. TARGET SELECTION BY CATEGORY

3.1. General SEGUE Target-Selection Principles

SEGUE targets are selected primarily from photometry in the *ugriz* SDSS filter system (Fukugita et al. 1996). For a few categories (cool WD, K giant, and M subdwarf candidates), the presence (or absence) and amplitude of a proper motion measurement from a match to an astrometric catalog (Munn et al. 2004; Lépine 2008) is also used.

The broad science goal of characterizing large-scale stellar structures in the Galaxy, combined with the specific goal of studying halo streams, informed the target-selection algorithms' design. The additional goals of finding rare but scientifically interesting samples of objects of unusually low metallicity, odd spectral type, or extreme kinematics were also factors.

The variety of science goals dictated a target-selection algorithm that sampled stars at a variety of distances, favoring those at large distances. The SEGUE Survey targets objects at a variety of colors and apparent magnitudes to probe distances from 10 pc (with WDs and M and K dwarfs) to the outer halo at $d \sim 100$ kpc (with BHB and red K giant stars). At intermediate distances, a target-selection category denoted "G star" (which contains some G IV subgiants) is sampled over the entire SEGUE magnitude range $14.5 < r_0 < 20.2$, and effectively probes the thick disk to inner halo transition region around the Galaxy with a large, unbiased sample.

SEGUE targets were divided into 15 different target categories, which spanned the range from the bluest (WD) to reddest (spectral type L brown dwarfs). Table 5 lists the SDSS/SEGUE Primary target bit in hexadecimal in Column 3. A search of the database may be done for objects with Primtarget matching these bits in the SpecObjAll table of the CAS (see below). The fourth column of Table 5 lists the magnitude, color, and proper motion cuts for each target type. When more stars than fibers in a given category are available for targeting, weighting mechanisms are used to subselect from candidates within a given category. These weighting mechanisms generally were designed to randomly subselect from all possible stars in a given category in a given 7 deg^2 field, with the probability of selection weighted by either magnitude (favoring brighter objects over fainter) or by color (favoring blue objects over red, except in the case of K giants). The colors used for target selection were in some cases generalized linear combinations of the SDSS *ugriz* generated colors. These generalized colors were designed to run parallel to or perpendicular to the color–color space stellar locus of (dereddened) Galactic stars (Lenz et al. 1998; Helmi et al. 2003). There is a maximum number of targets accepted in any given pointing in each category (see Column 5 of Table 5 which lists the maximum number of targets allowed per pointing, the approximate total number targeted by category during SEGUE, and a rough estimate of the fraction of the spectra in each category that turn out to be of the type that was targeted).

The SEGUE target-selection algorithms were not perfected immediately, and for some of the categories, several versions of the algorithm exist, as indicated in Column 2 of Table 5. The final version of SEGUE target selection is designated v4.6, with earlier revisions having lower version numbers. The significant changes from earlier versions of the target-selection cuts for each target type are tabulated, also in Table 5. Table 6 indicates the range of SEGUE plate numbers which correspond to each version of SEGUE target selection.

In general, colors of all objects are dereddened by their full Schlegel et al. (1998) extinction value before applying the various target-selection cuts described in Table 5 and below. Exceptions to this are the white dwarf/main-sequence (WD/MS) binary, the esdM, and the legacy brown dwarf and legacy WD categories, where applying the full dust correction, assuming the star lies behind the dust screen, is not correct, and thus uncorrected colors are preferred.

For each pointing, candidate lists of all objects which match the color and reduced proper motion cuts for each of the 15 categories are generated. Each of the 15 candidate lists is then sorted, usually randomly, but by magnitude in some cases (red K giants, low-metallicity categories). After guide stars, blank sky patches and spectrophotometric and reddening standards are assigned hole positions on each plate, science target assignment begins in a round-robin fashion: the lists of possible objects in each of the 15 categories are examined in turn and the first object in each list is assigned a fiber (assuming no 55″ collision with prior targets). After selecting a target from the

Table 5
SEGUE Selection by Target Type

Target Type	Version	PrimTargBits	Mag,Color,PM Cuts	Num/PP,Cand.,f
WD/sdO/sdB	v4.6	0 × 80080000	$g < 20.3, -1 < g-r < -0.2, -1 < u-g < 0.7, u-g+2(g-r) < -0.1$	25,4069,0.62
	v3.0		$-1 < u-g < 0.7, u-g+2(g-r) < -0.1$	
	v2.0		$g < 20.3, -1 < g-r < 0.2, -1 < u-g < 0.5$	
CWD	v4.6	0 × 80020000	$r < 20.5, -2 < g-i < 1.7$[b], $H_g > 16.05 + 2.9(g-i)$	10,1187,0.005
	v3.1		Allowed number of targets/pointing to exceed 10 on occasion	
	v3.0		$r < 20.5, -2 < g-i < 1.7, H_g > 16.05 + 2.9(g-i)$	
	v2.0		$15 < r20, -0.1 < g-r < 1.1, g-r > 2.4(r-i)+0.5, i-z < 0$	
BHB/BS/A	v4.6	0 × 80002000	$g < 20.5, 0.8 < u-g < 1.5, -0.5 < g-r < 0.2, v$[c]weight	150,24688,0.66
	v3.3		Added v "Luminosity color" weighting	
	v3.2		Sort by color, favor bluest BHBs	
	v3.0		$0.6 < u-g < 1.4, -0.5 < g-r < 0.2$	
	v2.0		$g < 20.5, 0.5 < u-g < 1.4, -0.8 < g-r < 0.2, s < -0.065$	
F	v4.6	0 × 80100000	$g < 20.3, -0.7 < P1(s)$[d] $< -0.25, 0.4 < u-g < 1.4, 0.2 < g-r < 0.7$	200,37900,0.68
	v3.0		$-0.7 < P1(s) < -0.25, 0.4 < u-g < 1.7, 0.2 < g-r < 3$	
	v2.0		$g < 20.3, -0.7 < P1(s) < -0.3, 0.4 < u-g < 1.7, -0.3 < g-r < 3$	
Low Metal	v4.6	0 × 80010000	$r < 19, -0.5 < g-r < 0.75, 0.6 < u-g < 3.0, l$[e] > 0.135	150,29788,0.12
	v3.4		Changed l-color cut to $l > 0.135$	
	v3.3		Changed l-color cut to $l > 0.15$	
	v3.1		Weighted by l-color and magnitude (bright targets favored)	
	v3.0		$r < 19.5, -0.5 < g-r < 0.75, l > 0.12$	
	v2.0		$r < 20.2, -0.5 < g-r < 0.9, 0.3 < u-g < 3, l > 0.15$	
F/G	v4.6	0 × 80000200	$g < 20.2, 0.2 < g-r < 0.48$	50,6939,0.9
	v3.3		First appearance of F/G category	
G	v4.6	0 × 80040000	$r < 20.2, 0.48 < g-r < 0.55$	375,62784,0.96
	v3.0		$0.48 < g-r < 0.55$	
	v2.0		$r < 20.2, 0.50 < g-r < 0.55$	
K giant	v4.6	0 × 80004000	$r < 18.5, 0.5 < g-r < 0.8$	70,16866,0.3
			l[e] > 0.07, pm < 11 mas yr^{-1}	
	v4.2		$g < 19.5, 0.5 < g-r < 0.9$	
	v3.0		$0.35 < g-r < 0.8, l > 0.07$, pm < 11 mas yr^{-1}	
	v2.0		$r < 20.2, 0.7 < u-g < 4, 0.4 < g-r < 1.2, 0.15 < r-i < 0.6, l > 0.1$	
	vt.t		$r < 20.2, 0.5 < g-r < 1.3$	
Red K giant	v4.6	0 × 80004000	$r < 18.5, 0.8 < g-r < 1.2$, pm < 5mas yr^{-1}	30,5948,0.08
	v4.4		$g < 18.5$, weight brighter, redder objects higher	
	v4.3		$g < 19.5, 0.9 < g-r < 1.2$	
AGB	v4.6	0 × 80800000	$r < 19.0, 2.5 < u-g < 3.5, 0.9 < g-r < 1.3$, s[f] < -0.06	10,1343,0.08
dK, dM	v4.6	0 × 80008000	$r < 19, 0.55 < g-r < 0.75$	50,18358,0.80
	v3.0		$r < 19.0, 0.55 < g-r < 0.75, 0.3 < r-i < 0.8$	
	v2.0		$r < 19.5, g-r > 0.7, 0.3 < r-i < 0.8$	
sdM	v4.6	0 × 80400000	$r < 20, g-r > 1.6, 0.9 < r-i < 1.3$	25,1012,0.003
esdM[a,g]	v4.6	0 × 81000000	$(g-r)0.787 - 0.356 > (r-i), r-i < 0.9, H_r > 17, 2.4 > g-i > 1.8$	40,9420,0.20
WD/MS[a]	v4.6	0 × 80001000	$g < 20, (u-g) < 2.25, -0.2 < g-r < 1.2, 0.5 < r-i < 2.0$	5,431,0.56
			$g-r > -19.78(r-i)+11.13, g-r < 0.95(r-i)+0.5$	
			$i-z > 0.5$ for $r-i > 1$	
			$i-z > 0.68(r-i)-0.18$ for $r-i < 1$	
	v3.4		Algorithm uses nondereddened colors	
	v3.3		First appearance MS/WD category	
L[h]	v4.6	0 × 80200000	$z < 19.5, i-z > 1.7$	5,1277,0.07
			$u > 21$	
	v3.0		Hi-z QSO style flag checks added	
LL Blue[i]	v4.6	0 × 80000800	$g-r < 0.25$	800,8522,0.3
	v4.0		First appearance all low-latitude algs	
LL AGB	v4.6	0 × 88000000	s[f] $> -0.13, 3.5 > u-g > 2.6, 0.8 < g-r < 1.3$	50,499,0.3
LL KIII	v4.6	0 × 80000400	$0.55 < g-r < 0.9, g < 19$, pm < 11 mas yr^{-1}	300,3220,0.3

Notes.
[a] For this category, colors and magnitudes are NOT dereddened.
[b] If neighbor with $g < 22$ within $7'\,'$, else $g-i < 0.12$.
[c] $v = -0.283(u-g) - 0.354(g-r) + 0.455(r-i) + 0.766(i-z)$, $-0.3 < g-r < 0.1$, gravity sensitive color for BHB/BS separation.
[d] $P1(s) = 0.91(u-g) + 0.415(g-r) - 1.28$.
[e] $l = -0.436u + 1.129g - 0.119r - 0.574i + 0.1984$, $0.5 < g-r < 0.8$.
[f] $s = -0.249u + 0.794g - 0.555r + 0.234$.
[g] The quoted color cuts are approximate.
[h] Additional flag checks are performed.
[i] This cut varies with reddening.

Table 6
Versions of SEGUE Target Selection

Version	Plate Range
vt.t	1660–1858
v2.0	1880–1919
v2.1	1960–1963
v3.0	2038–2077
v3.1	2147–2163
v3.2	2174–2302
v3.3	2303–2338
v3.4	2377–2476
v4.0	2534–2549
v4.2	2550–2741
v4.3	2796–2837
v4.4	2848–2877
v4.6	2887–2965

fifteenth category, the algorithm returns to the first category and the process repeats until all fibers are assigned. Categories are eliminated from consideration for target assignment when they reach their maximum fiber allocation or when there are no more candidates on a given list. This allows the categories with only a few targets per plate pair (cool WD, sdM, brown dwarf) to always have their candidates targeted, while several large categories (BHB, F, low-metal candidates, G, K giant) take up the bulk of the fibers on each plate pair.

The overall picture of where target categories are located in color and proper motion space is shown in Figure 3. The $(g-r)_0$ optical color can be used as proxy for effective temperature, and it provides a reasonable estimate of spectral type. For a star with proper motion μ in arcsec yr^{-1}, we define a reduced proper motion in the g filter: $H_g = g + 5\log\mu + 5$.

Targets are selected as PRIMARY detections (duplicates and objects from overlapping scans removed) of objects in the DR7 database with stellar (not extended) PSFs (the "STAR" table in the database). Candidates are required to pass the following SDSS flag cuts on the quality of their photometric imaging data. Objects must not be saturated (flag bit: SATURATED), must be close to the EDGE, must not have an interpolated PSF (INTERP_PSF), and must not have an inconsistent flux count (BADCOUNTS). In addition, if the center is interpolated (INTERP_CENTER), there should not be a cosmic ray (CR) hit indicated. These flags are set by the PHOTO pipeline for every object, and details on all possible flags, and their meaning can be found on the SDSS Web site: http://www.sdss.org. A few categories below, such as the L brown dwarf category, require stricter flag cuts.

We now give details of each target-selection algorithm by category, as summarized in Table 5, and present representative spectra of the various target types. The sample spectra are plotted with flux in units of 10^{-17} erg cm^{-2} s^{-1} Å on the y-axis versus wavelength in Å on the x-axis. If more than one spectrum appears in a plot, then additional spectra are offset by an arbitrary amount for readability. Spectra are smoothed from 1.5 to three 150 km s^{-1} resolution elements, depending on the S/N. Common spectral features are indicated by line name (and the occasional night-sky feature by "NS"). Spectra are labeled with their unique SDSS/SEGUE three-part ID (plate-mjd-fiberId), as well as with relevant magnitudes, colors, or atmospheric quantities from the SSPP analysis. All example spectra, along with their measured parameters, can be found in the DR7 data release by using their three-part ID to look them up.

3.2. White Dwarfs, sdB, sdO

WDs are important for absolute calibration of the astrophysical temperature and flux scales, including calibration of filter systems that span ultraviolet (UV), optical, and IR wavelengths (Holberg & Bergeron 2006; Bohlin 2007). The SDSS WD catalogs of Kleinman et al. (2004) and Eisenstein et al. (2006) contain an extensive list of WDs discovered in the SDSS imaging and spectroscopy.

A goal of SEGUE is to continue this survey of hot WDs by obtaining spectra of most WDs with $T > 14000$ K and most hot subdwarf stars, while excluding most QSOs. SEGUE obtained spectra of 4069 hot WD candidates, of which about 62% appear to be DA type WDs while roughly 15% are other types of WDs. Other hot stars, designated sdB and sdO types (Green et al. 1986), most of which are extreme horizontal branch stars, are also selected by this SEGUE WD color box. Roughly 10% of the objects selected as hot WD targets are QSO or emission-line galaxy contaminants. Figure 4 shows sample SEGUE DA WD, sdB, and sdO spectra.

3.3. Cool White Dwarfs

Cool WD stars, the fossil remains of an ancient stellar population, offer a window into the early stages of the Galaxy and its formation. They can be used to place lower limits on the ages of various Galactic components, extend our knowledge of stellar evolution, and provide hints of star formation processes during the Galaxy's earliest epochs. Very cool (ultracool) WDs with hydrogen in their atmospheres exhibit a unique spectral signature due to collision-induced absorption (CIA) by molecular hydrogen. In pure H-atmosphere WDs, CIA is mediated by H_2–H_2 collisions that produce a flux suppression in the IR at temperatures below about 5000 K, resulting in objects of very unusual color.

SDSS has proven to be an excellent database in which to search for ultracool WDs. To date, 14 new ultracool WDs have been discovered in SDSS spectral data (Harris et al. 2001, 2008; Gates et al. 2004; Hall et al. 2008), constituting the majority of known ultracool WDs. Additional cool WD candidates have been identified in SDSS photometric data (Kilic et al. 2006; Vidrih et al. 2007). Several extremely faint high proper motion cool WDs have recently confirmed in the SDSS repeat-scan (stripe 82) data (Scholz et al. 2008).

SEGUE presents a unique opportunity to find more of these rare objects. Recent SDSS studies of WDs (Kilic et al. 2006; Harris et al. 2006) have demonstrated the usefulness of a reduced proper motion cut for selecting candidates from the photometric data, and a similar procedure is used to identify targets in the SEGUE imaging data. Objects which satisfy the Table 5 selection cuts in color and reduced proper motion are targeted as cool WDs and assigned spectral fibers. All selected targets are required to have a good proper motion match (as defined in Kilic et al. 2006) in order to obtain a reliable reduced proper motion H_g.

For target-selection versions prior to v3.3, cool WDs were allotted a maximum of 10 fibers per plate pair; however, analysis of preliminary SEGUE data observed in 2004 revealed that selection cuts frequently yielded fewer than this, with occasional fields containing 11–15 target objects while the overall average remained less than 10. As a result the final target-selection algorithm targets all objects which satisfy the selection criteria (increasing the number of ultracool WD fibers to more than 10 if necessary for a specific plate pair), ensuring that we obtain

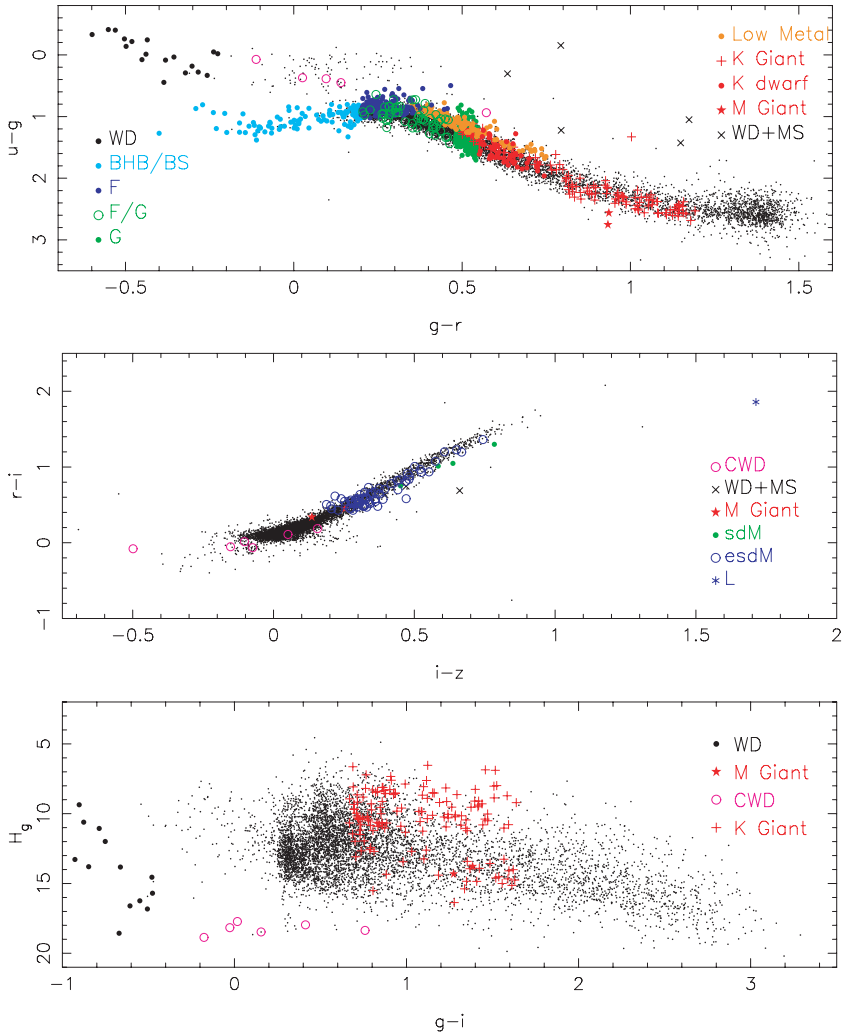

Figure 3. SEGUE target selection at a glance—target-selection categories in SEGUE. Top panel: $(g-r)_0$, $(u-g)_0$ color–color diagram showing different SEGUE target categories in different colors/symbols. Note the "Low Metal" category hugs the blue side (in $(u-g)_0$) of the stellar locus, and a substantial fraction of F stars with redder $(u-g)_0$ and $0.2 < (g-r)_0 < 0.48$ are not targeted, except by the F/G category. Middle panel: the same as above, except categories which use redder $(i-z)_0$, $(r-i)_0$ colors are highlighted. Note the L dwarf candidate at $(i-z, r-i)_0 = (1.72, 1.9)$. The proper motion selected extreme M subdwarf candidates are shown as open blue circles. Lower panel: a $(g-i)_0$, H_g selection diagram for categories which use USNO-B proper motion in their selection. $H_g = g + 5\log_{10}(\mu/1000) + 5$, where μ is the proper motion in mas yr^{-1}. Note the cool WD candidates (high proper motion) as magenta circles and the K giant candidates (consistent with 0 proper motion).

spectra for all candidates. This reduced proper motion selection algorithm also allows us to target all low-luminosity WDs and most high-velocity WDs and identify cool WD candidates that exhibit milder CIA suppression.

SEGUE targeted about 1187 cool WD candidates. While an analysis of the full SEGUE cool WD set is currently underway, preliminary results show that the selection by reduced proper motion is yielding a high return of cool and high-velocity WDs. Out of 16 plate-pairs studied, 60% of the targets are cool DA type WDs, 18% are DQ or DZ type, and 12% are DC type, while 10% are contaminating objects of nondegenerate stars or QSOs. Of the rare ultracool WDs that are intended as a goal of this selection category, two of the 15 published SDSS ultracool WDs (SDSS J0310-01 and SDSS J2239+00) were targeted in this category and found in early SEGUE spectra. Figure 5 shows a sample cool WD spectrum from SEGUE.

3.4. BHB, A Main Sequence, Blue Stragglers

BHB stars in the halo are important distant standard candles for mapping structure in the outer halo (Yanny et al. 2000). They may be seen to distances of 80 kpc or more and, along with red K giants, are our most distant stellar halo probe of kinematics (Newberg et al. 2003). The recent work of Xue et al. (2008) shows how this sample probes large enough distances in the halo to constrain the mass of the Milky Way at $d \sim 50$ kpc. A linear combination of the SDSS colors, $v = -0.283(u-g) - 0.354(g-r) + 0.455(r-i) + 0.766(i-z)$ (Lenz et al. 1998) is somewhat helpful in separating BHBs from higher surface gravity blue stragglers (BS), and it is used to weight the selection of targets toward BHBs. BS are surprisingly common in the halo, and are thought to be the result of binary evolution. They are an interesting population in their own right, though halo members can be difficult to separate from disk populations at brighter magnitudes (Momany et al. 2007). SEGUE placed fibers on 24,688 BHB/BS candidates, and about 66% of the resulting spectra are auto-classified as BHB/BS types. Figure 6 shows examples of BHB and BS spectra.

3.5. F Turnoff, Plate Spectrophotometric Standards

F turnoff stars are an extremely numerous, relatively luminous category, and their spectra are very clean and amenable to

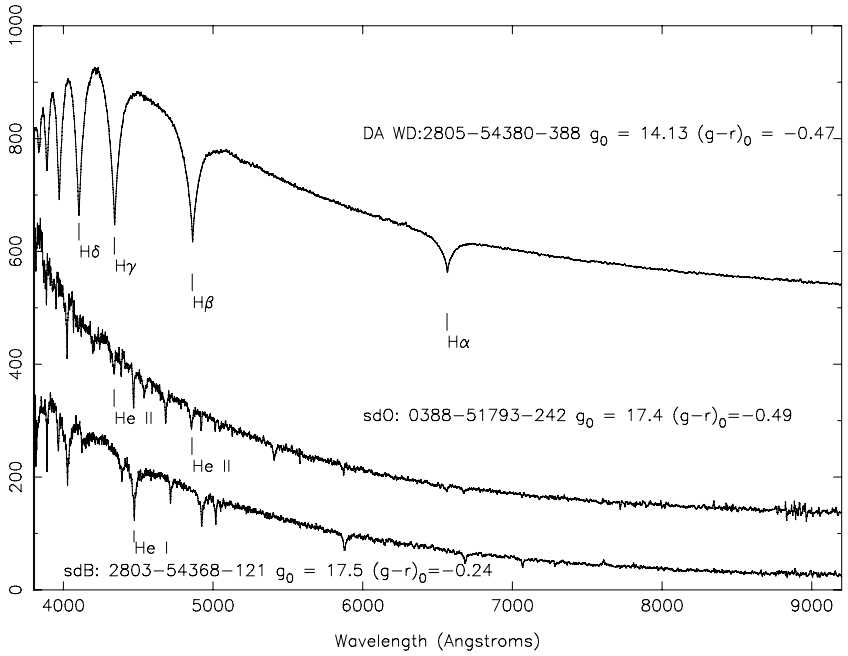

Figure 4. WD—top: a sample SEGUE DA (hydrogen) WD; middle: a candidate sdO star showing a characteristic hot spectrum; lower: a candidate sdB star, which have colors similar to the WD.

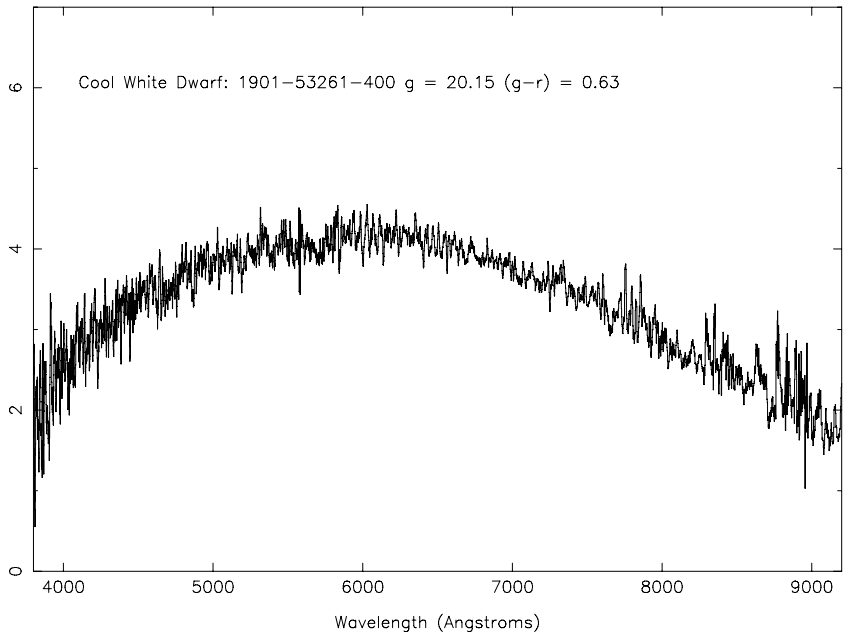

Figure 5. CWD—a sample SEGUE cool WD where CIA due to H_2 has removed flux redward of 6000 Å, leaving a spectrum with very unusual colors.

accurate spectroscopic analysis (Ramírez et al. 2006). The number of F turnoff stars available toward a given SEGUE pointing far exceeds the number of fibers available, thus, in targeting this category, SEGUE used linear combinations of the $((u-g)_0,(g-r)_0)$ colors to favor the selection of lower metallicity, halo objects. This is done by using the "s" (perpendicular to the stellar locus) and P1(s) (parallel to stellar locus) colors as described in Helmi et al. (2003). These colors essentially "straighten-out" the stellar locus in the vicinity of the turnoff and allow a simple cut on P1(s) to favor halo subdwarfs, even as the relative density of thick disk versus halo turnoff stars is changing rapidly as a function of magnitude. For stars with $g < 19$, the S/N is generally high enough for the SSPP to derive atmospheric parameters with relatively small uncertainties. In the faintest magnitude bin ($19 < g < 20.5$), only the RVs are still accurate, but it is possible to use this large number of F dwarfs to probe halo substructure at distances of $10 < d < 18$ kpc from the Sun (Newberg et al. 2002, 2007). Due to their large numbers and relative absolute brightnesses, SEGUE targeted 37,900 F subdwarfs, plus about 6500 spectrophotometric and reddening standards. About 70% of these candidates yielded spectra classified as type F, with some indication of lower metallicity ([M/H] < -0.7).

Kinematics of SEGUE F turnoff stars has recently allowed Willett et al. (2009) to tightly constrain the orbit of a halo stream (Grillmair & Dionatos 2006).

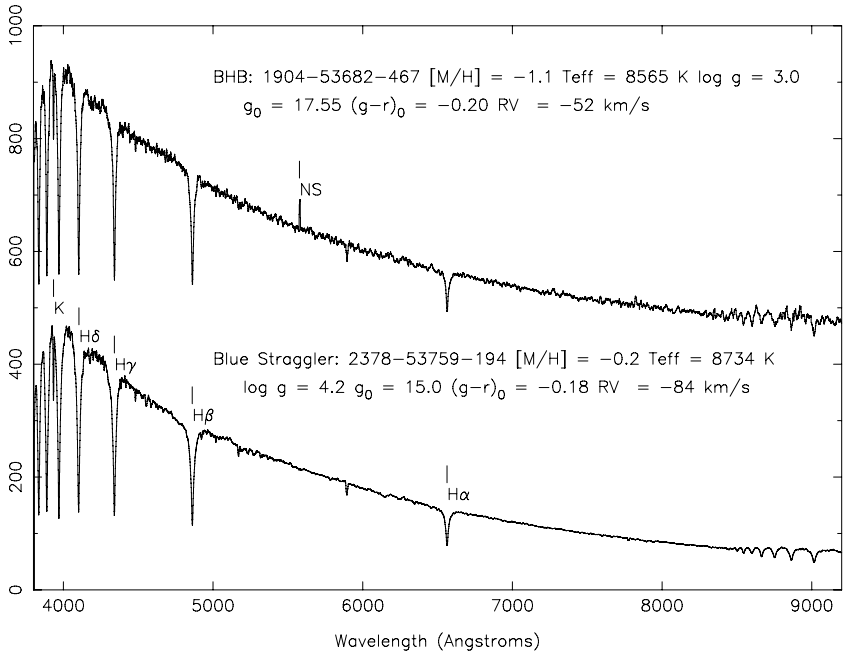

Figure 6. BHB/BS—Upper: a sample SEGUE BHB star. Note the low surface gravity, log $g = 3.0$, deep and narrow Balmer lines characteristic of this type. Lower: a sample SEGUE BS star. Note the somewhat broader Balmer lines, the strong Paschen series lines in the IR, and the higher measured surface gravity log $g = 4.2$.

3.6. Low-Metallicity Candidates

The $u - g$ color of F, G, and K stars with $0.4 < (g-r)_0 < 0.8$ can be used as a metallicity proxy, in the sense that bluer stars tend to have lower metallicity (Lenz et al. 1998). We can employ this color cut to restrict the number of spectroscopic targets. For $(g - r)_0 > 0.8$, $(u - g)_0$ fails as an effective discriminant.

Another item to consider when searching for very low metallicity stars is the volume sampled. While low-metallicity K and M dwarf stars live for much longer on the main sequence than F and G stars, their intrinsic faintness relative to the other spectral types means that our magnitude-limited sample of these stars is dominated by disk stars that are near the Sun. Relatively few spheroid stars are expected to be observed in the small volume of the Galaxy that we probe with late type dwarfs. Since F "turnoff" stars are significantly brighter (they can be 1–2 mag brighter than their zero-age main-sequence luminosity), and therefore can be seen to further distances, many of the lowest metallicity [Fe/H] < -3.0 candidate objects identified to date have been found to have colors of F turnoff stars. See Allende Prieto et al. (2008) and Carollo et al. (2007) for extensive studies of halo F turnoff stars.

SEGUE targeted 30,998 candidates in the low-metallicity category. About 12% (4600) of them show an SSPP metallicity of [M/H] < -2. About 0.1% (32) indicate metallicity [M/H] < -3. The very lowest metallicity candidates will need to be follow-up on larger telescope at higher resolution. We show in Figure 7 a set of turnoff stars, all with similar effective temperatures, that have metallicities ranging from [M/H] < -3 to super-solar (the higher metallicity stars in this sequence were not selected from the low-metallicity targeting category).

It should be noted that the present version of the SSPP, described in detail by Lee et al. (2008a, 2008b), Allende Prieto et al. (2008), and Re Fiorentin et al. (2007) produces conservative estimates of [Fe/H] for stars with metallicities below roughly [Fe/H] $= -2.7$. A recent preliminary analysis of over 80 SDSS/SEGUE stars with SSPP metallicity determinations [Fe/H] < -2.7, based on high-resolution spectroscopy obtained with the Subaru/HDS (W. Aoki 2008, private communication), indicates that the actual metallicity can be 0.3 dex lower than the level determined by the SSPP. This analysis shows that the lowest metallicity stars from this category have [Fe/H] $= -3.7$. With this new recalibration, T. C. Beers et al. (2009, in preparation) assemble some 15,000 stars with [Fe/H] < -2.0, and several hundred with [Fe/H] < -3.0. These totals include low-metallicity stars from all of the various target categories used in SDSS/SEGUE.

3.7. F/G Stars

The F/G target category represents an unbiased random subsampling of the range of stars with colors $0.2 < (g - r)_0 < 0.48$. This distinguishes it from the F subdwarf category (above), which is biased toward objects of lower metallicity. This category was only used in target-selection versions v3.3 and later. SEGUE targets 6939 of these, of which 90% are classified as type F or G. Figure 8 shows an example spectrum.

3.8. G Dwarfs and Sgr Subgiants

The G dwarf sample represents SEGUE's largest single homogeneous stellar spectral category. The target selection is very simple, just a color cut in $(g - r)_0$, and thus is very close to unbiased. With the SEGUE unbiased G dwarf sample, researchers will be able to address the metallicity distribution function (MDF) as well as the kinematic distribution of G dwarfs in a much larger volume of the Galaxy than has been previously attempted (Wyse & Gilmore 1995; Wyse 1986).

This sample will also be extremely useful for probing the structure of the Galaxy's major components, especially using the brighter stars with S/N > 20, for which surface gravities can be determined by the SSPP. Subgiant stars (spectral type G IV) stars in the Sagittarius dwarf tidal debris stream can also be isolated from stars in this selection category.

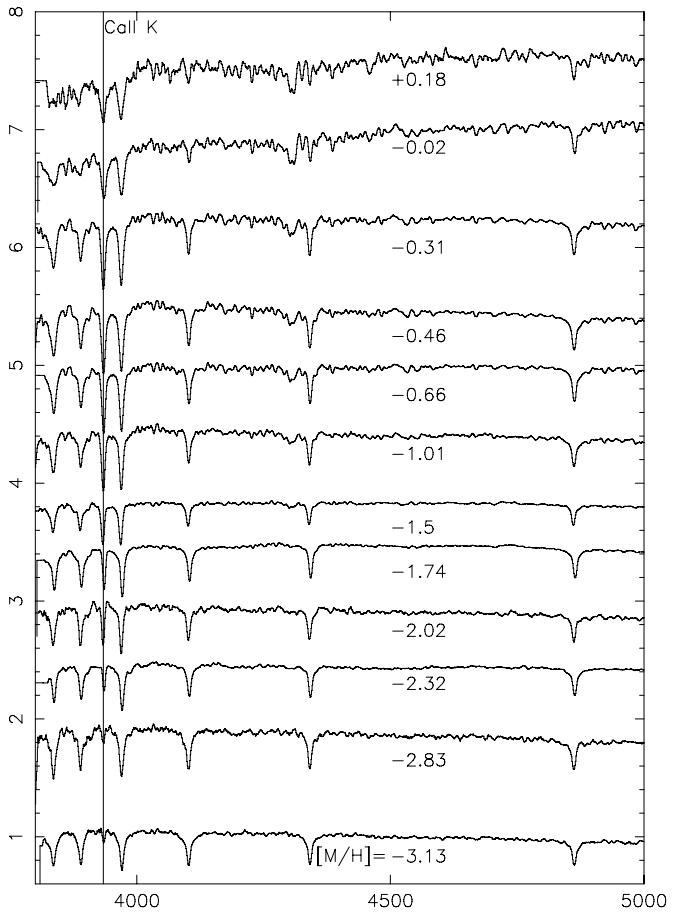

Figure 7. F star metal sequence—a set of SEGUE F stars, selected to show the range of metallicities sampled by the F subdwarf, F/G, spectrophotometric standard and reddening standard categories. All 13 stars have similar effective temperatures, near 6500 K, but the strength of the Ca K line at λ3933 indicates metallicities ranging from less than 0.001–1.5 times Solar.

SEGUE targeted 62,784 G star candidates based on the simple color selection. At least 96% of these yield G star spectra. A significant population (roughly 7%) of evolved (subgiant or giant) spectra are indicated by the SSPP $\log g < 3.75$ indicator. Figure 9 shows a sample G dwarf star spectrum (lower) and a G giant spectrum (upper).

3.9. K Giants

K giants are the most luminous tracers available for old stellar populations. They can (albeit rarely) be found with absolute magnitudes M_g as high as −2.0. Such stars at $g = 18$ are then located at a distance of 100 kpc.

It is not possible to use a simple selection criterion such as that used by SEGUE for F/G stars or G dwarfs to select K giants, because in SEGUE's apparent magnitude range, giants are swamped in number by foreground dwarfs with the same $(g - r)$ color. We can use the G dwarf category, which overlaps the blue edge of the K giant color range, to demonstrate this. Only 3% of the targeted G dwarf stars with $g = 15$–17 in the SEGUE data are giants. By contrast, 50% of the stars with similar magnitudes that were targeted with the selection criteria described below are giants.

In past surveys, K giants have been identified using the pressure-sensitive feature near 5200 Å produced by a blend of the Mg I*b* triplet and the MgH band, which is strong in dwarfs and weak in giants, but unfortunately also has some sensitivity to stellar metallicity and temperature (Seitter 1970). This feature is a good luminosity criterion for late G and K stars redward of $(g - r)_0 = 0.5$ ($B - V \sim 0.75$). Ratnatunga & Freeman (1985) and Flynn & Morrison (1990) used objective prism spectra to isolate stars with weak Mg*b*/H features in the G/K color range. As it is quite a broad feature, it is also possible to measure their strength using intermediate-band photometry (Morrison et al. 2000).

Since the SDSS *ugriz* filters do not have a narrow filter in the Mg*b*/H region, we use a more indirect method of finding giants. In SEGUE's magnitude range, many of the giants that we observe are halo stars, so we use a photometric metallicity indicator to remove foreground disk dwarfs. Briefly, we select stars with a UV-excess in the *ugriz* system, and use the power of our fiber spectroscopy to eliminate the remaining foreground dwarfs.

In more detail, in the $(g - r)_0$, $(u - g)_0$ diagram, metal-poor stars appear bluer in $(u - g)_0$ for a given $(g - r)_0$ because they have less line-blanketing in the *u* filter. Two different colors have been defined to measure the deviations from the mean stellar locus in this diagram: the *s*-color of Helmi et al. (2003) and the *l*-color of Lenz et al. (1998). Large values of the *l*-color correspond to metal-poor stars, and we have chosen to target stars with $l > 0.07$. Our selection strategy is complicated by the fact that the Mg*b*/MgH feature is within the SDSS *g* passband (it is in the blue wing of the *V* filter). Giants (with weaker Mg*b*/MgH) will be bluer in $g - r$ than dwarfs.

Figure 10 shows how the competing effects of metallicity and gravity play out. Our K giant selection region extends from $(g - r)_0 = 0.5$ to 1.2. The main locus, from the accurate averaged photometry from Stripe 82 (Ivezić et al. 2007) is shown in gray: stars with *l*-color greater than 0.07 are shown in light gray. Spectroscopically confirmed dwarfs are shown with large crosses, and giants with large filled circles. Giants range in metallicity from near solar to [Fe/H] less than −2.0. It can be seen that for $(g - r)_0$ between 0.5 and 0.8, the metallicity sensitivity of the $(u - g)_0$ color is the dominant effect, and metal-weak giants are clustered toward the blue side of the locus. For redder stars, the luminosity sensitivity of $(g - r)_0$ dominates, and giants appear above the main locus.

The details of our target selection for this category have changed as we have learned more about the behavior of giants, particularly the rare red giants and dwarfs in *ugriz* colors, particularly the rare red giants. The efficiency of our discovery of K giants depends on magnitude and color. Using an *l*-color cut of 0.10 rather than 0.07, success rates are as follows: for $g = 17$–18, $0.5 < (g - r)_0 < 0.6$, our success rate is 45%. For the same magnitude range and $0.6 < (g - r)_0 < 0.8$, the success rate is 28%.

A modification to the K giant algorithm occurred for SEGUE target-selection version v4.2 and later to extend the selection to very red ($0.8 < (g-r)_0 < 1.2$) K giants, which are referred to as red K giants in the SEGUE target-selection tables (there are few bona fide M giant spectra, with TiO bands and $(g-r)_0 > 1.3$, in SEGUE). Although only the last quarter or so of SEGUE plates targeted very red K giants, 5948 fibers were placed on these very red stars, of which 466 (8%) yielded a low-gravity spectral indicator from SSPP. The selection algorithm included $(g - r)_0$ color, lack of proper motion, and a weighting toward brighter magnitudes. For effective random sampling with only a proper motion cut for $(g - r)_0$ between 0.8 and 1.2, the success rate is 2.5%.

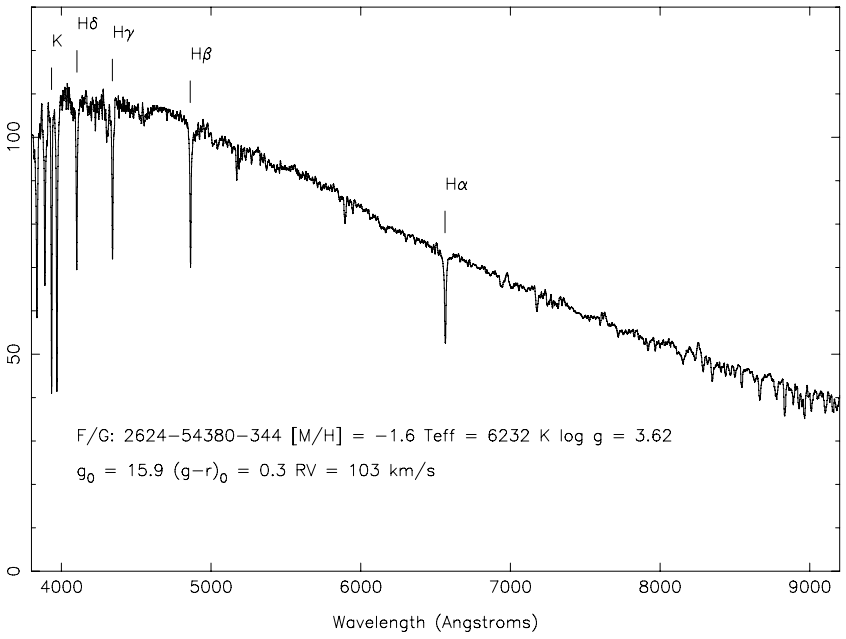

Figure 8. FG—a sample SEGUE F/G star. This category samples with only a simple $(g-r)_0$ color cut, and is therefore nearly unbiased.

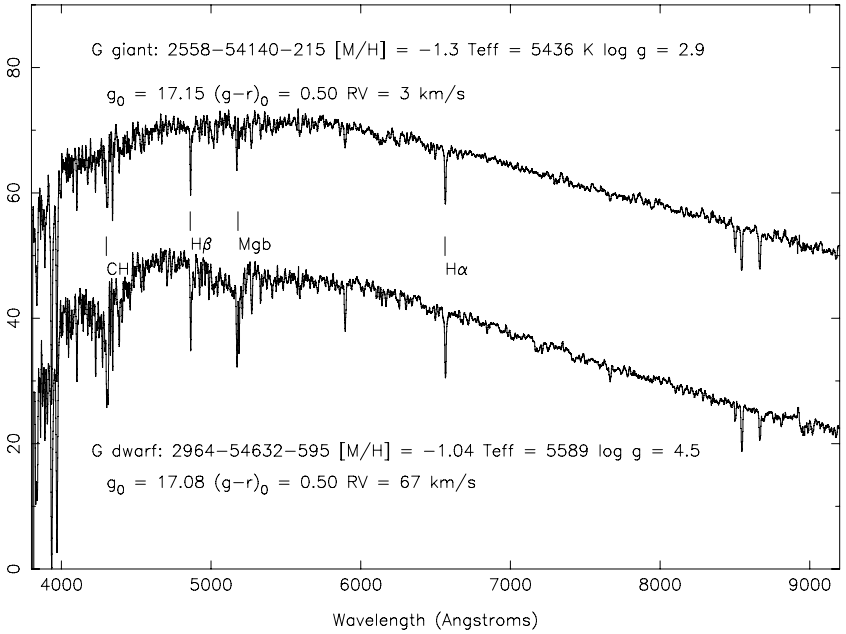

Figure 9. G—Upper: the weak M*g*/H feature at λ5140 indicates that this G star is actually a higher luminosity evolved subgiant, on its way up the red giant branch. Approximately 7% of the SEGUE G star sample shows low surface gravity. Lower: a more typical G dwarf star.

This important category received 22,814 fibers, of which about 30% yielded a low surface gravity K giant, red K giant, or subgiant spectrum. Figure 11 shows a classic K giant (top panel) and a very red K giant (lower panel).

3.10. AGB

An early SEGUE target-selection category, designated "asymptotic giant branch (AGB)," that was intended to select the very reddest giants in Figure 10, targeted 1343 objects. Only about 8%, however, yielded actual red giant (and possible AGB) spectra. In hindsight, the choice of *s*-color cuts, and $(g-r)_0$ limits were not optimal, and the low-latitude AGB category, (LL AGB) below, and the red K giant category above eventually superseded this AGB category for SEGUE target selection of this type of object.

3.11. K Dwarfs, Early M Dwarfs

The K dwarf and early M dwarf category generated a significant unbiased sample of relatively nearby Galactic objects with complete six-dimensional phase-space information: proper motions, RVs, positions, and photometric parallax distance estimates are all available for this data set. SEGUE targeted 18,358 stars in this category, of which 80% yield useful spectra. Figure 12 shows sample K and M dwarfs.

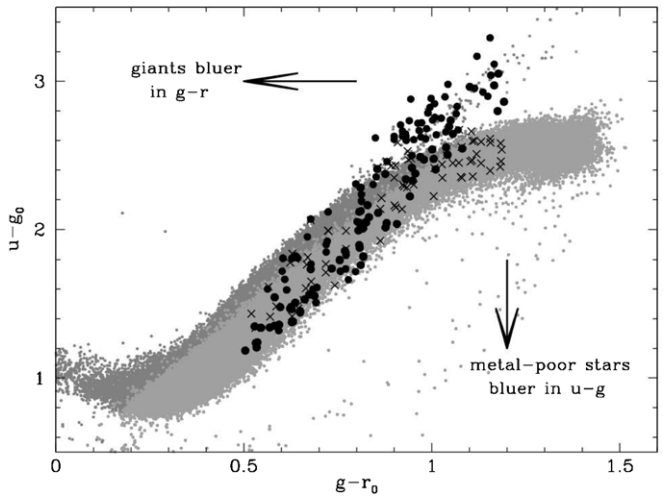

Figure 10. Red giant selection—a demonstration of how the K giant locus crosses from the blue ($u - g$) side of the stellar locus at $g - r = 0.6$ over to the red side of the locus at $g - r = 1.0$. M giants with TiO features appear at $g - r > 1.3$ and $u - g > 3.0$. The small dot shows the photometric stellar locus in a SEGUE high-latitude field (there are Sagittarius M giants present at the end of the locus). Stars with l-color greater than 0.07 are shown in light gray. Spectroscopically confirmed dwarfs are shown with large crosses, giants with large filled circles.

3.12. M Subdwarfs, High Proper Motion M Stars

The aim of this category is to obtain a sample of low-metallicity M (sub)dwarfs, which are strongly correlated with halo M dwarfs. Originally, 1012 sdMs were targeted, based on a version of the West et al. (2008) color cuts. However, for a variety of reasons, only a handful of these candidates were actual sdMs. A second window onto this category was opened by using the American Museum of Natural History (AMNH) high proper motion catalog and careful color selection criteria (Lépine 2008; Lépine & Scholz 2008). Approximately, 40 fibers per plate pair were allocated to this search for sdM, esdM, and usdM objects. This category obtained a very high (∼20%) success rate on an allocation of 9420 candidate fibers. Figure 13 shows a low metal M dwarf and a high proper motion selected extreme subdwarf M star (esdM2.5).

3.13. WD/MS Binaries

This category, designated WD/MS binary, has been used successfully to improve our understanding of close compact binary evolution. If the SEGUE WD/MS Survey is combined with follow-up observations identifying the short orbital period systems among the WD/MS binary stars, important processes such as the common envelope phase (see Webbink 2007, for a recent review) or angular momentum loss by magnetic wind braking can be constrained (see Politano & Weiler 2006; Schreiber et al. 2007). Already, SDSS-I efficiently identified new WD/MS binaries. Smolcic et al. (2004) identified a new stellar locus, the WD/MS binary bridge. Silvestri et al. (2006, 2007) published lists of more than 1400 spectroscopically identified WD/MS binaries. These samples, however, mainly consisted of young systems containing hot WDs.

The selection criteria used here have been designed to identify a large sample of old WD/MS binaries containing cold WDs that, according to Schreiber & Gänsicke (2003), should represent the dominant population of WD/MS binaries. On 240 spectroscopic plates in DR7, the WD/MS color selection algorithm chose 9531 candidates of which 431 have been observed spectroscopically. Among these we confirm 244 WD/MS objects (with 25 other possible candidates) resulting in a success rate of ∼56%. A first analysis shows that indeed for the first time a large sample of old systems with WD temperatures below ∼12,000 K could be identified (for more details, see M. R. Schreiber et al. 2009, in preparation). Follow-up observations to further constrain compact binary evolution are well underway (Rebassa-Mansergas et al. 2007, 2008; M. R. Schreiber et al. 2009, in preparation; A. Schwope et al. 2009, in preparation). The total SEGUE allocation to this WD/MS category is about 500 fibers, with a 56% success rate expected. Figure 14 shows one example WD/MS spectrum.

3.14. Brown Dwarfs, L, and T Dwarfs

Very red objects are photometrically detected in the z image, but not in the bluer $ugri$ SDSS images. These are rare and interesting objects, and the only difficulty in targeting them was to assure that the one detection was a solid detection and not a spurious CR hit to the z-band CCD. Additional flag checking was performed for candidates in this category, similar to that done by Fan et al. (1999) for selecting very high redshift quasars that are detected in i, z or z only. SEGUE devoted 1277 fibers to this category, with about a 7% initial estimated yield of objects with spectral type later than M8. Figure 15 shows a SEGUE L dwarf spectrum.

3.15. The Low-Latitude (LL) Algorithms

For 12 pointings at $|b| < 20$ (all toward regions of high reddening, $E(B-V) > 0.3$), the previously mentioned SEGUE target-selection algorithms were not effective. The long lines of sight through the Galactic disk, at low latitudes, often rendered invalid the implicit assumption that all of the dust lies *in front* of the target stars. For these pointings, marked as "LLSurvey" in Table 3, we use an alternative target-selection scheme that targeted three categories: (1) bluest object candidates (mostly BHB and F stars): selecting the bluest ($g - r$) objects in any given pointing without regard for absolute colors; (2) K giant candidates: using the absence of proper motion as the primary selection criterion; and (3) AGB type objects: singling out objects in a fashion similar to that used for selecting red K giants, but with a brighter g magnitude limit. This latter category was assigned only a small fraction of fibers.

Because of dust and crowding, recovering the selection function at low latitudes is problematic, and optical spectrophotometry of these low-latitude stars with SEGUE should be regarded as experimental, with an eye toward future surveys.

About 12,241 fibers were devoted to low-latitude algorithm plates. Each of the three primary LL categories, K giant (3220 candidates), AGB (499 candidates), and Blue-tip (8522 candidates) yielded about 30% success rate based on SSPP analysis using methods which fit normalized spectra (flattened without continuum slope, and are thus much less dependent on reddening). Figure 16 shows three spectra from one LL algorithm plate, one from each category.

3.16. The SDSS Legacy Stellar Target-Selection Algorithm

In addition to SEGUE, the SDSS and SDSS-II Legacy Surveys obtained spectra for nearly 200,000 (additional) stars, which were allocated fibers on the main SDSS Legacy Survey

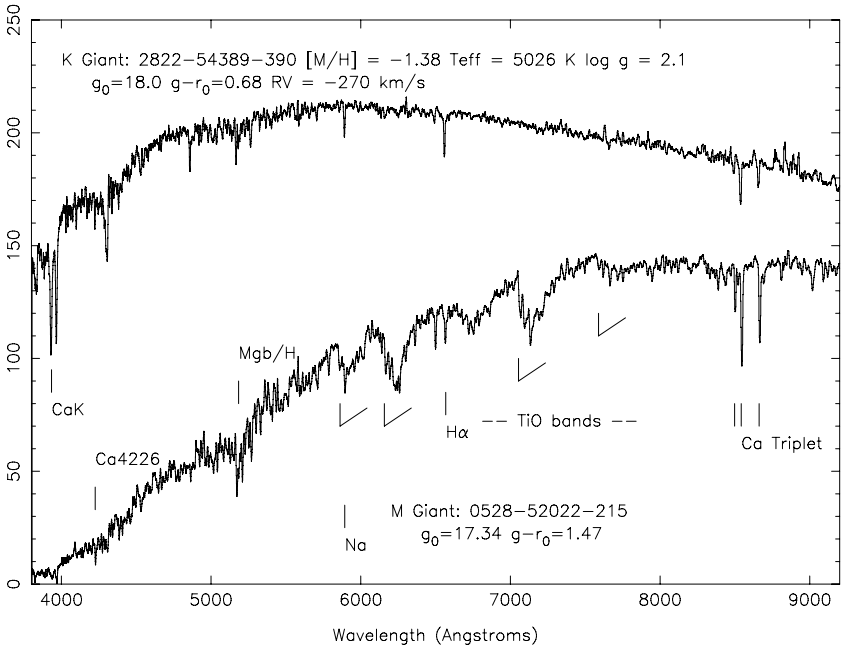

Figure 11. KIII—Top: a sample SEGUE K giant star, weak Mg*b*/H feature, the weak Ca 4226 and the weak Na I λ5890. Bottom: a sample SEGUE red K giant star. Even though this spectrum shows strong TiO bands, usually found in early M dwarfs, it is clearly a giant, due to its relatively weak Mg*b*/H, nearly absent Na I λ5890, weak Ca λ4226, and strong Ca IR triplet. This star has an absolute $M_g = -1$ and is at a distance of 45 kpc from the Sun in the Sagittarius tidal stream's Northern leading tail.

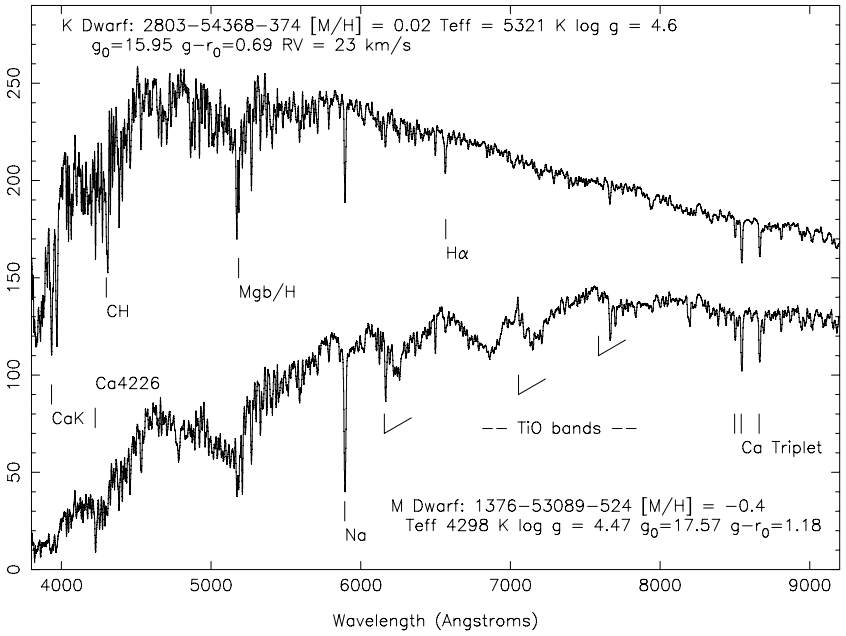

Figure 12. KV—Top: a sample SEGUE K dwarf, note the strong Mg*b*/H and Na I. Lower: a sample SEGUE M dwarf, note the strong MgH, Na I, and TiO molecular bands.

plates that observed primarily galaxies. The target-selection categories were briefly described in Stoughton et al. (2002). We list in Table 7 the color and magnitude cuts used to select stars by category in the SDSS Legacy Survey. It should be noted that, unlike SEGUE, Legacy's stars targeting algorithms may assign multiple target type bits to the same target, that is, an object may be targeted based on its colors, as both a SERENDIPITY_RED object and a ROSAT_E object. These bits are tabulated in the PrimTarget field of the CAS database. The final column of Table 7 lists the approximate number of candidates which received a fiber in each target category.

3.17. Cluster Plates

In order to calibrate the SSPP's metallicity, luminosity, and effective temperature scales for all stars, a significant number of known globular clusters and a few open clusters were targeted with one or more SEGUE plates. These 12 pointings are indicated with the cluster name followed by the word "Cluster" in Table 3. Because many of these clusters are relatively nearby, they have giant branches with stars brighter than the SEGUE spectroscopic saturation limit of $r \sim 14$. Additionally, due to the extreme density of the globular cluster fields, even the

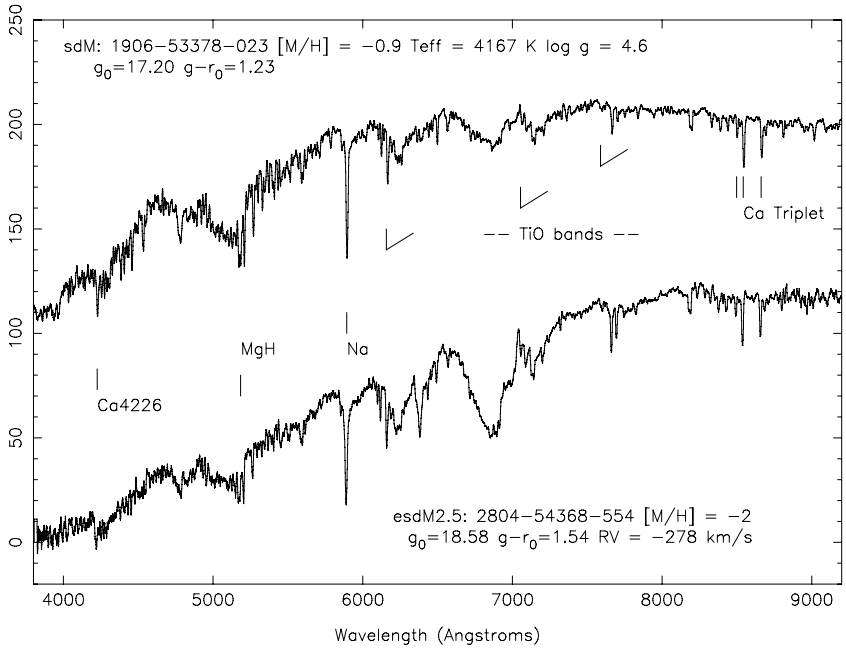

Figure 13. sdM—a sample SEGUE M subdwarf, the SEGUE estimate of metallicity is uncertain at these cool temperatures. An AMNH proper motion and color-selected SEGUE esdM2.5 extreme subdwarf. Note that the TiO bands are nearly gone.

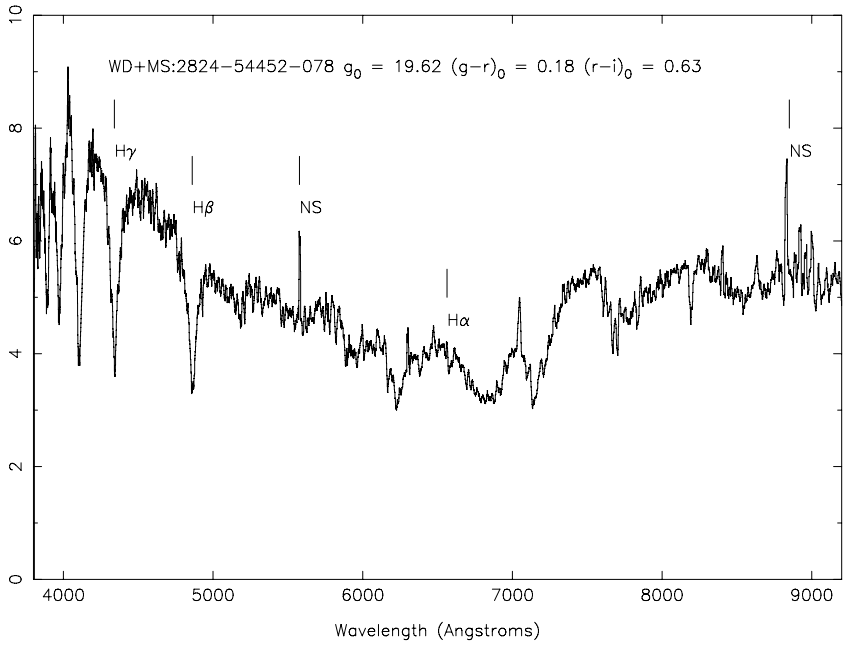

Figure 14. WD/MS—a sample SEGUE WD plus MS binary. Stellar parameters determined from modeling the SEGUE data are a WD of $T_{\rm eff} \sim 19000$ K, a WD mass of $\sim$0.6 $M_{\odot}$, and a spectral type M4 for the companion.

Pan-STARRS assisted PHOTO processing of SDSS and SEGUE imaging scans failed to resolve individual stars in the centers of the globulars. For these reasons, the following procedures were followed for most cluster plate observations. (1) The target list for each cluster was generated individually. Proper motion membership criteria were used for many clusters, allowing the targeting of stars in the dense cores of clusters which were saturated in the regular SDSS imaging. K. Cudworth (2006, private communication) provided membership lists for a significant fraction of the clusters targeted. Some of these targets do not, therefore, have standard SDSS run–rerun–camcol–field–id numbers, and are identified only by their R.A., decl. positions. (2) Shorter exposures were obtained for many of the clusters. One or two minute exposures allowed us to obtain nonsaturated spectra of stars as bright as $r \sim 11$.

These cluster spectra were used to calibrate the SSPP for all types of stars (Lee et al. 2008a, 2008b). The spectra of cluster stars are available on an "as is" basis in the DR7 database. Users should be aware that the spectrophotometry and in some cases the RV solutions of these plates may be subject to large systematic errors due to the extremely short exposure times, and that occasional bright targets may be saturated.

A major effort to process SDSS and SEGUE imaging data for clusters has been undertaken by An et al. (2008), using

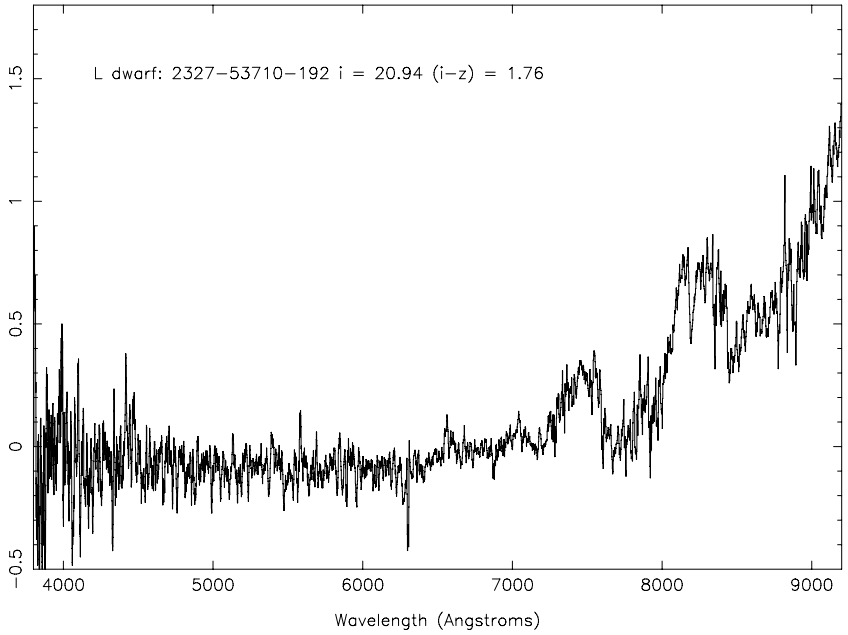

Figure 15. L—a sample SEGUE brown dwarf of approximate spectral type L0 (or M9). The *u*, *g*, and *r* band flux is nearly completely missing from these objects.

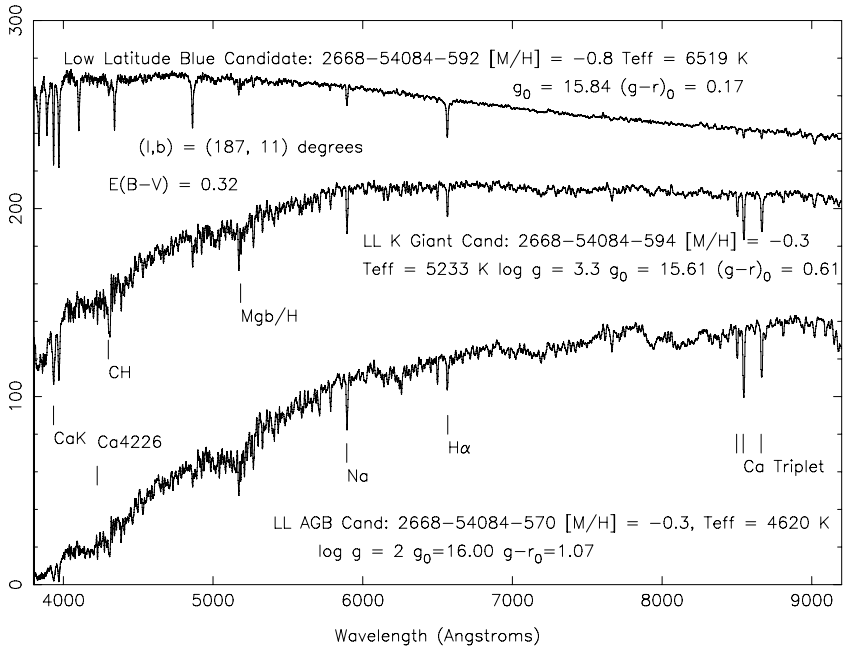

Figure 16. Low-latitude selected objects—a sample of three SEGUE low-latitude target-selection objects from the same SEGUE plate. Upper: a blue-tip candidate object, clearly of spectral type F. Middle: a K giant candidate. Lower: a candidate AGB object.

the DAOPHOT/ALLFRAME suite of programs. They reduced imaging data for crowded cluster fields where PHOTO did not run, and presented accurate photometry for 20 globular and open clusters.[36] This effort has led to fiducial sequences for clusters over a wide range of metallicities in the SDSS *ugriz* filter system.

3.18. Special Plates Centered on Halo Substructure

Studying halo streams is an important goal of SEGUE, and SEGUE is well placed to obtain new kinematic information on the stars in these streams. Five previously known streams were specially targeted at various positions along their extent with SEGUE plates, for a total of 16 pointings. The five streams are Sagittarius (Yanny et al. 2000), Monoceros (Newberg et al. 2002), Orphan (Belokurov et al. 2007b), Virgo (Vivas et al. 2001; Juric et al. 2008), and GD-1 (Grillmair & Dionatos 2006). Plates with these pointings are marked with the stream name and "Strm" in Table 3. The regular target-selection algorithms described above were used on these streams, i.e., no special targets within the stream were given specific fibers. Some BHB, BS, F turnoff, K giant, and G subgiant spectra are clearly confirmed stream members on these "Strm" plates. Identification of a particular star as a stream member versus a field star is of course, often difficult, and left to the interested researcher.

[36] Available at http://www.sdss.org/dr7/products/value_added/anjohnson08_clusterphotometry.htm

Table 7
Legacy Stellar Target Selection by Type

Target Type	PrimTargBits	Mag,Color,PM Cuts	Cand.[a]
SPECTROPHOTO STD	0×20	$0.1 < g-r < 0.4, 16 < g < 17.1$	20320
REDDEN STD	0×2	$0.1 < g-r < 0.4, 17.1 < g < 18.5$	22337
HOT STD	0×200	$g < 19, u-g < 0, g-r < 0$	3370
ROSAT C	0×800	$r < 16.5$ ROSAT X-ray source within 60″	8000
ROSAT C	0×800	$u-g < 1.1$ ROSAT within 60″	
ROSAT E	0×8000000	ROSAT within 60″	8000
STAR BHB	0×2000	$-0.4 < g-r < 0, 0.8 < u-g < 1.8$	19887
STAR CARBON	0×4000	$g-r > 0.85, r-i > 0.05, i-z > 0, r-i < -0.4+0.65(g-r)$	4453
		$(g-r) > 1.75$	
STAR BROWN DWARF	0×8000	$z < 19, \sigma(i) < 0.3, r-i > 1.8, i-z > 1.8$	667
STAR SUBDWARF	0×10000	$g-r > 1.6, 0.95 < r-i < 1.6, \sigma(g) < 0.1$	1482
STAR CATY VAR[b]	0×20000	$g < 19.5, u-g < 0.45, g-r < 0.7, r-i > 0.3, i-z > 0.4$	8959
	0×20000	$(u-g)-1.314(g-r) < 0.61, r-i > 0.91, i-z > 0.49$	
STAR RED DWARF	0×40000	$i < 19.5, \sigma(i) < 0.2, r-i > 1.0, r-i > 1.8$	14649
STAR WHITE DWARF	0×80000	$g-r < -0.15, u-g+2(g-r) < 0, r-i < 0$	6059
		$H_g^c > 19, H_g > 16.136+2.727(g-i)$	
		$g-i > 0, H_g > 16.136+2.727(g-i)$	
STAR PN	0×10000000	$g-r > 0.4, r-i < -0.6, i-z > -0.2, 16 < r_0 < 20.5$	20
SERENDIP BLUE	0×100000	$u-g < 0.8, g-r < -0.05$	81937
SERENDIP FIRST	0×200000	FIRST radio source within 1″.5	14689
SERENDIP RED[b]	0×400000	$r-i > 2.7, i-z > 1.6$	4179
SERENDIP DISTANT[b]	0×800000	$g-r > 2, r-i < 0$	11820

Notes.
[a] An object may be a Legacy target in multiple categories.
[b] For this category, colors and magnitudes are NOT dereddened.
[c] $H_g = g + 5\log(\mu) + 5$, μ in arcsec yr^{-1}.

4. THE DATA ARCHIVE AND AN EXAMPLE QUERY

All of the spectra and associated imaging from SEGUE were made public as a part of DR7 of the SDSS-II Survey on 2008 October 31. The calibrated magnitudes and positions of objects as determined by the SDSS PHOTO pipeline software are available in the "photoobjall" and "star" tables of the CAS database, which is available through interfaces at http://cas.sdss.org and described in detail at http://www.sdss.org. We note that the SEGUE and SDSS Legacy imaging and spectra are all in a single large database, so it is possible to obtain SDSS Legacy photometry and SEGUE spectroscopic information for stars in the SDSS and SDSS-II footprints as part of a single query, or closely related set of queries. The SSPP and SPECTRO outputs (RV, [M/H], $\log g$, $T_{\rm eff}$) are available in tabular form in the "sppParams" and "specObjAll" tables of the CAS database. FITS format files containing all of the ∼240,000 extracted, co-added, sky-subtracted, flux-calibrated spectra are available at http://das.sdss.org for interested researchers. Similar files for all 200,000 stellar objects detected by SDSS and SDSS-II Legacy Surveys are also available at the same location.

To highlight the usefulness of the data archive, we present an example SQL query from the CAS database to help construct plots showing the extent and scientific usefulness of SEGUE data.

We design a query to select SEGUE-targeted G stars from the database, and return each object's photometric and tabulated spectroscopic information.

The following SQL query is presented to the CAS DR7 database (http://cas.sdss.org/CasJobs):

```
select dbo.frun(targetid) as run,
dbo.frerun(targetid) as rerun,
dbo.fcamcol(targetid) as camcol,
dbo.ffield(targetid) as field,
dbo.fobj(targetid) as obj,
g0,umg0,gmr0,spp.ra,spp.dec,spp.l,spp.b,
spp.plate,spp.mjd,spp.fiberid,elodierv,
elodierverr,
feha,fehaerr,fehan, logga,loggaerr,
elodierv+10.1*cos(b*3.14159/180)*
cos(l*3.14159/180)+
224.0*cos(b*3.14159/180)*sin(l*3.14159/180)+
6.7*sin(b*3.14159/180) as vgsr from
sppParams spp,specobjall sp,
platex p where spp.specobjid = sp.specobjid
and sp.plateid =
p.plateid and p.programname like 'SEGUE%' and
gmr0 between 0.48 and 0.55
and elodierverr > 0
```

This query is written in "SQL," a standard database query language. Some details of the query are as follows.

The first six lines select photometric quantities for the desired objects, include the unique five-part SDSS imaging ID (run,rerun,camcol,field,obj), dereddened photometry (g_0, $(u-g)_0$, $(g-r)_0$), (R.A.,decl.) J2000, and Galactic (l, b).

The next three lines select spectroscopic outputs for each object: unique three-part SDSS/SEGUE spectroscopic ID (plate,mjd,fiberid), RV and error (obtained by cross-correlation with ELODIE RV templates), *elodierv*, *elodierverr* in km s^{-1}, and SSPP estimates of [M/H] (feha) with error (fehaerr) and an indication of how many estimators went in to the [M/H] estimate (fehan). Similarly, the stellar surface gravity and error is retrieved (logga, loggaerr).

A significant fraction of the spectra will have feha or logga set to −9.999, which indicates that the SSPP did not have sufficient S/N to estimate this value confidently. These values are mostly for fainter $g > 19$ spectra.

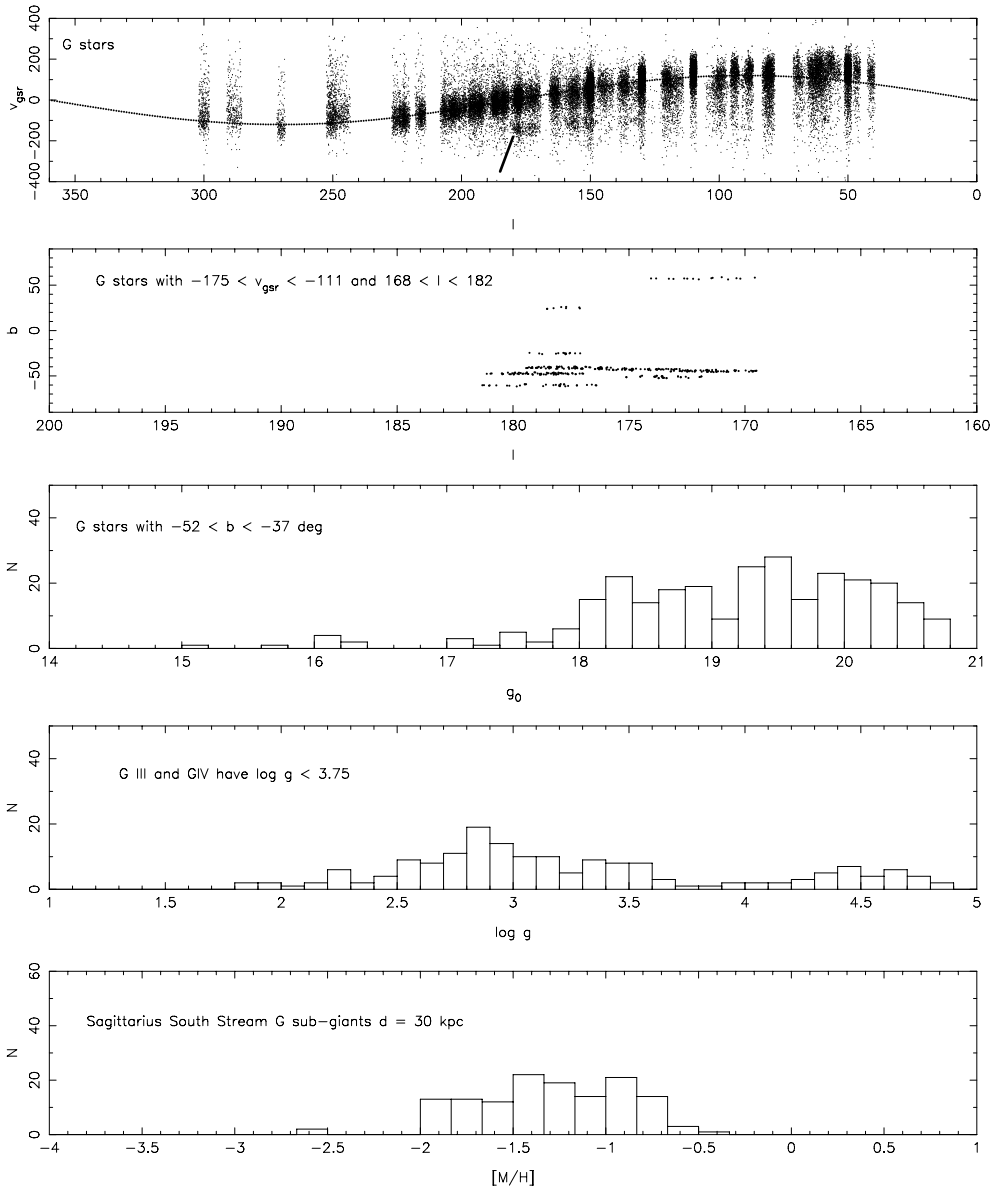

Figure 17. Sample Query—the five panels here show a step-by-step analysis of the SEGUE G star spectroscopic sample to isolate an interesting subpopulation. Top: $(l, v_{\rm gsr})$ plot of 61,343 measured SEGUE G star parameters from the CAS database. A sinusoidal line, representing a rotating thick disk population is indicated with a black curve. Subsets of stars which stand out from the black curve are candidate halo dwarf galaxy or stream structures. A feature of interest for further study is highlighted with a black mark pointing to $(l, v_{\rm gsr}) = (170^\circ, -160\,{\rm km\ s^{-1}})$. There are several other interesting features which will not be explored further here. Second from top: the set of stars selected in $(l, v_{\rm gsr})$ is plotted in (l, b) to localize the interesting structure in position on the sky. Middle: the magnitude distribution of these stars is quite broad, centered near $g \sim 19$, but covering in excess of a 2 mag range. It is possible that they are all at the same approximate distance only if we are sampling a steep subgiant branch population. Second from bottom: a histogram of the SSPP measured surface gravity of this sample indicates that nearly all these objects ($\log g < 3.75$) are in fact subgiants rather than dwarfs. Bottom: the metallicity distribution of these objects indicates a metallicity of [M/H] $= -1.4 \pm 0.5$, with individual object errors on metallicity of about 0.3. The implied distance to these objects, if they are one population, is about 30 kpc. The spatial location of these objects is consistent with previous studies of the Sagittarius tidal stream Southern trailing tail.

The next lines take each object's heliocentric RV and Galactic (l, b) and uses the database to compute the Galactocentric $v_{\rm gsr}$ velocity using standard values for the solar motion.

The selection is done with an SQL "join" between the SSPP table "sppParams," and the spectroscopic id table "specobjall" and the plate list table "platex," requiring that the type of spectroscopic program matches the key phrase "SEGUE" (to exclude LEGACY SDSS galaxy plates) and that the dereddened color of the objects fall in the G dwarf color range ($0.48 < (g - r)_0 < 0.55$). Additionally, the RV error must be greater than zero, indicating a minimal level of quality of the spectrum. This also excludes galaxies and quasars, leaving only objects with stellar kinematics.

This query yields a table (in comma separated value format, which may be downloaded to a user's local computer for further manipulation) of 61,343 objects.

Individual images of spectra in this data set may be examined by fetching from the DAS, with a link like

```
wget
http://das.sdss.org/spectro/1d_26/1880/gif/
spPlot-53262-1880-014.gif
```

where the object may be verified to be a G star.

A FITS data file of the calibrated 1D spectrum is available from

```
wget
http://das.sdss.org/spectro/1d_26/1880/
1d/spSpec-53262-1880-014.fit
```

for detailed further manipulation.

Figure 17 shows steps in isolating an interesting subpopulation of these G stars. The topmost panel plots Galactic $v_{\rm gsr}$ versus l for all G stars selected with the CAS database query above. A sinusoidal curve with amplitude 120 km s^{-1} shows the average path of stars rotating with the Sun about the Galactic center. Several knots of G stars stick out from the general disk population(s). We focus on one set of stars with $-175 < v_{\rm gsr} < -111$ km s^{-1} and $168^\circ < l < 182^\circ$. Galactic (l, b) for this subset is plotted in the second panel. A histogram of the apparent magnitudes of the further subset of stars with $-52^\circ < b < -37^\circ$ is plotted in the third panel. If these stars are dwarfs at $M_g \sim 5.5$, their implied distance from the Sun is 5 kpc. However, they may be giants or subgiants at much further distances. We plot the histogram of SSPP surface gravities in panel 4. There is a clear peak at subgiant and giant $\log g < 3.75$ (all G dwarfs have $\log g > 4.25$). Therefore, this population consists of subgiants with $M_g \sim 1.5$, placing the stars at $d = 30$ kpc from the Sun. A histogram of the quantity feha (adopted average [Fe/H] from the SSPP pipeline) for the subgiants is shown in the lowest panel. The estimated metallicity of these objects is [M/H] $= -1.4 \pm 0.5$. The location of these objects on the sky and their implied distances and velocities are consistent with that of Sagittarius Southern tidal stream stars, such as RR Lyraes and BHBs seen in Ivezić et al. (2000) and Yanny et al. (2000).

This example just scratches the surface of the interesting science that can be obtained with the SEGUE G star sample.

5. SUMMARY

The SEGUE Survey provides a large sample of more than 240,000 spectra of stars at $(14 < g < 20.3)$ covering 212 sightlines out to distances of 100 kpc. It supplements the SDSS Legacy imaging survey with an additional 3500 deg^2 of *ugriz* imaging at $|b| < 35^\circ$. Each 7 deg^2 sightline obtains 1150 well-calibrated resolution $R = 1800$ spectra, analyzed by a uniform set of software pipelines to generate tables of RVs for all stars and estimates of [Fe/H], $\log g$, and $T_{\rm eff}$ for stars with S/N > 10. The selected targets in each pointing cover all major spectroscopic types from WDs to L brown dwarfs in numbers sufficient to sample the kinematic structure of all major stellar components of the Galaxy (except the bulge) at distances from the solar neighborhood (probed with M, L, and T dwarfs) to 100 kpc from the Sun (probed with BHB and K/M giant stars). The SEGUE sample is useful for isolating stellar substructures, particularly in the stellar halo.

The unbiased sample of over 60,000 G dwarf spectra presents a unique way to study the Galaxy's structure in detail. Selected populations of rare targets ranging from cool WDs to high proper motion subdwarf M stars to stars with metallicity [M/H] < -3 allow theories of formation and evolution of the Milky Way to be newly constrained.

A follow-up to the SEGUE Survey, entitled SEGUE-2, is now underway with the same instrument and telescope configuration and aims to obtain targeted spectra of a sample of similar size and quality to SEGUE.

All SEGUE data are calibrated and publicly accessible, now enabling a segue to many productive science explorations beyond the dreams of the designers.

Funding for the SDSS and SDSS-II has been provided by the Alfred P. Sloan Foundation, the Participating Institutions, the National Science Foundation, the U.S. Department of Energy, the National Aeronautics and Space Administration, the Japanese Monbukagakusho, the Max Planck Society, and the Higher Education Funding Council for England. The SDSS Web site is http://www.sdss.org/.

The SDSS is managed by the Astrophysical Research Consortium for the Participating Institutions. The Participating Institutions are the American Museum of Natural History, Astrophysical Institute Potsdam, University of Basel, Cambridge University, Case Western Reserve University, University of Chicago, Drexel University, Fermilab, the Institute for Advanced Study, the Japan Participation Group, Johns Hopkins University, the Joint Institute for Nuclear Astrophysics, the Kavli Institute for Particle Astrophysics and Cosmology, the Korean Scientist Group, the Chinese Academy of Sciences (LAMOST), Los Alamos National Laboratory, the Max-Planck-Institute for Astronomy (MPIA), the Max-Planck-Institute for Astrophysics (MPA), New Mexico State University, Ohio State University, University of Pittsburgh, University of Portsmouth, Princeton University, the United States Naval Observatory, and the University of Washington.

C. Allende Prieto acknowledges support from NASA grants NAG 5-13057 and NAG 5-13147. T. C. Beers, Y. S. Lee, and S. Thirupathi acknowledge partial funding of this work from grant PHY 02-16783: Physics Frontiers Center/Joint Institute for Nuclear Astrophysics (JINA), awarded by the U.S. National Science Foundation. P. Re Fiorentin acknowledges support through the Marie Curie Research Training Network ELSA MRTN-CT-2006-033481. We acknowledge useful discussions with Steve Majewski on the G dwarf target-selection design. We acknowledge several useful suggestions from the referee.

REFERENCES

Abazajian, et al. 2009, ApJS, in press (arXiv:0812.0649)
Adelman-McCarthy, J., et al. 2008, ApJS,, 175, 297
Allende Prieto, C., et al. 2006, AJ, 636, 804
Allende Prieto, C., et al. 2008, AJ, 136, 2070
An, D., et al. 2008, ApJS, 179, 326
Becker, R. H., et al. 2001, AJ, 122, 2850
Beers, T. C., Preston, G. W., & Shectman, S. A. 1985, AJ, 90, 2089
Bell, E. F., et al. 2008, ApJ, 680, 295
Belokurov, V., et al. 2006a, ApJ, 642, L137
Belokurov, V., et al. 2006b, ApJ, 647, L111
Belokurov, V., et al. 2007a, ApJ, 654, 897
Belokurov, V., et al. 2007b, ApJ, 658, 337
Bidelman, W. P., & MacConnell, D. J. 1973, AJ, 78, 687
Blanton, M. R., Lin, H., Lupton, R. H., Maley, F. M., Young, N., Zehavi, I., & Loveday, J. 2003a, AJ, 125, 2276
Blanton, M., et al. 2003b, ApJ, 592, 819
Bohlin, R. C. 2007, in ASP Conf. Ser. 364, The Future of Photometric, Spectrophotometric and Polarimetric Standardization, ed. C. Sterken (San Francisco, CA: ASP), 315
Cameron, D., & Nassau, J. J. 1956, ApJ, 124, 346
Cannon, A. J., & Pickering, E. C. 1918, Ann. Harv. Coll. Obs., 91, 1
Carollo, D., et al. 2007, Nature, 450, 1020
Christlieb, N., Wisotzki, L., Reimers, D., Gehren, T., Reetz, J., & Beers, T. C. 1999, in ASP Conf. Ser. 165, The Third Stromlo Symposium: The Galactic Halo, ed. B. K. Gibson et al. (San Francisco, CA: ASP), 259
Edvardsson, B., Andersen, J., Gustafsson, B., Lambert, D. L., Nissen, P. E., & Tomkin, J. 1993, A&A, 275, 101
Eisenstein, D. J., et al. 2005, ApJ, 633, 560
Eisenstein, D. J., et al. 2006, AJ, 132, 676
Fan, X., et al. 1999, AJ, 118, 1
Fan, X., et al. 2003, AJ, 125, 1649
Flynn, C., & Morrison, H. L. 1990, AJ, 100, 1181
Frieman, J., et al. 2008, AJ, 135, 338

Fukugita, M., Ichikawa, T., Gunn, J. E., Doi, M., Shimasaku, K., & Schneider, D. P. 1996, AJ, 111, 1748
Gates, E., et al. 2004, ApJ, 612, L129
Gilmore, G., Wyse, R. F. G., & Jones, J. B. 1995, AJ, 109, 1095
Gilmore, G., Wyse, R. F. G., & Norris, J. E. 2002, ApJ, 574, L39
Green, R. F., Schmidt, M., & Liebert, J. 1986, ApJS, 61, 305
Grillmair, C., & Dionatos, O. 2006, ApJ, 643, L17
Gunn, J. E., & Stryker, L. L. 1983, ApJS, 52, 121
Gunn, J. E., et al. 1998, AJ, 116, 3040
Gunn, J. E., et al. 2006, AJ, 131, 2332
Hall, P. B., Kowalski, P. M., Harris, H. C., Awal, A., Leggett, S. K., Kilic, M., Anderson, S. F., & Gates, E. 2008, ApJ, 136, 76
Harris, H. C., et al. 2001, ApJ, 549, L109
Harris, H. C., et al. 2006, AJ, 131, 571
Harris, H. C., et al. 2008, ApJ, 679, 697
Helmi, A., et al. 2003, ApJ, 586, 195
Hogg, D. W., Finkbeiner, D. P., Schlegel, D. J., & Gunn, J. E. 2001, AJ, 122, 2129
Holberg, J. B., & Bergeron, P. 2006, AJ, 132, 1221
Houk, N. 1978, in Michigan Catalog of Two-dimensional Spectral Types for the HD Stars (Ann Arbor, MI: Department of Astronomy, Univ. of Michigan), QB6.H77
Ibata, R., & Gilmore, G. 1995, MNRAS, 275, 591
Ibata, R., Gilmore, G., & Irwin, M. J. 1994, Nature, 370, 194
Ivezić, Ž., et al. 2000, AJ, 120, 963
Ivezić, Ž., et al. 2007, AJ, 134, 973
Jacoby, G. H., Hunter, D. A., & Christian, C. A. 1984, ApJS, 56, 257
Juric, M., et al. 2008, ApJ, 673, 864
Katz, et al. 2004, MNRAS, 354, 1223
Kilic, M., et al. 2006, AJ, 642, 1051
Kleinman, S. J., et al. 2004, ApJ, 607, 426
Koposov, S., et al. 2007, ApJ, 669, 337
Kuijken Gilmore, G. 1989, MNRAS, 239, 651
Lee, Y. S., et al. 2008a, AJ, 136, 2022
Lee, Y. S., et al. 2008b, AJ, 136, 2050
Lenz, D. D., Newberg, H. J., Rosner, R., Richards, G. T., & Stoughton, C. 1998, ApJS, 119, 121
Lépine, S. 2008, AJ, 135, 2177
Lépine, S., & Scholz, R.-D. 2008, ApJ, 681, L33
Magnier, E. 2006, in The Advanced Maui Optical and Space Surveillance Technologies Conference, Wailea, Maui, HI, ed. S. Ryan, The Maui Economic Development Board, E50
Momany, Y., Held, E. V., Saviane, I., Zaggia, S., Rizzi, L, & Gullieuszik, M. 2007, A&A, 468, 973
Morgan, W. W., Keenan, P. C., & Kellman, E. 1943, An Atlas of Stellar Spectra, With an Outline of Spectral Classification (Chicago, IL: Univ. of Chicago Press), QB881.M6
Morrison, H. L., et al. 2000, AJ, 119, 2254
Moultaka, J., Ilovaisky, S. A., Prugniel, P., & Soubiran, C. 2004, PASP, 116, 693
Munn, J. A., et al. 2004, AJ, 127, 3034
Nassau, J. J., Stephenson, C. B., & Mc Connell, D. J. 1965, Luminous Stars in the Northern Milky Way (volume 6, Bergedorf: Hamburger Sternwarte and Warner & Swasey Observatory)
Newberg, H., Yanny, B., Cole, N., Beers, T. C., Re Fiorentin, P., Schneider, D. P., & Wilhelm, R. 2007, ApJ, 668, 221
Newberg, H., et al. 2002, ApJ, 569, 245
Newberg, H., et al. 2003, ApJ, 596, L191
Nordström, B., et al. 2004, A&A, 418, 989
Padmanabhan, N., et al. 2008, ApJ, 674, 1217
Patterson, R. J., Majewski, S. R., Kundu, A., Kunkel, W. E., Johnston, K. V., Geisler, D. P., Gieren, W., & Muñoz, R. 1999, BAAS, 31, 1439
Pickles, A. J. 1985, ApJS, 59, 33
Pier, J. R., Munn, J. A., Hindsley, R. B., Hennessy, G. S., Kent, S. M., Lupton, R. H., & Ivezic, Z. 2003, AJ, 125, 1559
Perryman, M. A. C., et al. 2001, A&A, 369, 339
Politano, M., & Weiler, K. P. 2006, ApJ, 641, L137
Ramírez, I., Allende Prieto, C., Redfield, S., & Lambert, D. L. 2006, A&A, 459, 613
Ratnatunga, K. U., & Freeman, K. C. 1985, ApJ, 291, 260
Re Fiorentin, P., Bailer-Jones, C. A. L., Lee, Y. S., Beers, T. C., Sivarani, T., Wilhelm, R., Allende Prieto, C., & Norris, J. E. 2007, A&A, 467, 1373
Rebassa-Mansergas, A., Gänsicke, B. T., Rodríguez-Gil, P., Schreiber, M. R., & Koester, D. 2007, MNRAS, 382, 1377
Rebassa-Mansergas, A., et al. 2008, MNRAS, 390, 1635
Richards, G., et al. 2006, AJ, 131, 2766
Rockosi, C., et al. 2002, AJ, 124, 349
Schlegel, D. J., Finkbeiner, D. P., & Davis, M. 1998, ApJ, 500, 525
Scholz, R.-D., Storm, J., Knapp, G. R., & Zinnecker, H. 2008, A&A, 494, 949
Schreiber, M. R., & Gänsicke, B. T. 2003, A&A, 406, 305
Schreiber, M. R., Nebot Gomez-Moran, A., & Schwope, A. D. 2007, in ASP Conf. Ser. 372, 15th European Workshop on White Dwarfs, ed. R. Napiwotzki & M. R. Burleigh (San Francisco, CA: ASP), 459
Seitter, W. C. 1970, in Atlas for Objective Prism Spectra, Bonner Spektral Atlas I (Bonn: Duemmler)
Silvestri, N. M., et al. 2006, AJ, 131, 1674
Silvestri, N. M., et al. 2007, AJ, 134, 741
Slettebak, A., & Brundage, R. K. 1971, AJ, 76, 338
Smith, J. A., et al. 2002, AJ, 123, 2121
Smolcic, V., et al. 2004, ApJ, 615, L141
Steinmetz, M., et al. 2006, AJ, 132, 1645
Stoughton, C., et al. 2002, AJ, 123, 485
Tegmark, M., et al. 2004, ApJ, 606, 702
Tremonti, C., et al. 2004, ApJ, 613, 898
Tucker, D., et al. 2006, Astron. Nachr., 327, 821
Vidrih, S., et al. 2007, MNRAS, 382, 515
Vivas, A. K., et al. 2001, ApJ, 554, L33
Webbink, R. F. 2007, in Short Period Binary Stars, ed. E. F. Milone, D. A. Leahy, & D. W. Hobill (Berlin: Springer), 233
West, A. A., Hawley, S. L., Bochanski, J. J., Covey, K. R., Reid, I. N., Dhital, S., Hilton, E. J., & Masuda, M. 2008, AJ, 135, 785
Wilkinson, M. I., et al. 2005, MNRAS, 359, 1306
Willett, B., Newberg, H. J., Zhang, H. T., Yanny, B., & Beers, T. C. 2009, ApJ, in press (arXiv:0901.4046)
Willman, B., et al. 2005, AJ, 129, 2692
Wyse, R. F. G. 1986, Nature, 322, 806
Wyse, R. F. G., & Gilmore, G. 1992, MNRAS, 257, 1
Wyse, R. F. G., & Gilmore, G. 1995, AJ, 110, 2771
Xu, Y., Deng, L. C., & Hu, J. Y. 2007, MNRAS, 379, 1373
Xue, X. X., et al. 2008, ApJ, 684, 1143
Yanny, B., et al. 2000, ApJ, 540, 825
Yanny, B., et al. 2003, ApJ, 588, 824
York, D., et al. 2000, AJ, 120, 1579
Zucker, D., et al. 2004a, ApJ, 612, L117
Zucker, D., et al. 2004b, ApJ, 612, L121
Zwitter, T., et al. 2008, AJ, 136, 421